PREEMACS: Pipeline for preprocessing and extraction of the macaque brain surface

Pamela Garcia-Saldivar [a], Arun Garimella [a,b], Eduardo A. Garza-Villarreal [a], Felipe A. Mendez [a], Luis Concha [a,*], Hugo Merchant [a,*]

[a] *Institute of Neurobiology, Universidad Nacional Autónoma de México, Campus Juriquilla. Blvd. Juriquilla, 3001 Querétaro, Querétaro, México*
[b] *International Institute of Information Technology, Hyderabad, India*

ABSTRACT

Accurate extraction of the cortical brain surface is critical for cortical thickness estimation and a key element to perform multimodal imaging analysis, where different metrics are integrated and compared in a common space. While brain surface extraction has become widespread practice in human studies, several challenges unique to neuroimaging of non-human primates (NHP) have hindered its adoption for the study of macaques. Although, some of these difficulties can be addressed at the acquisition stage, several common artifacts can be minimized through image preprocessing. Likewise, there are several image analysis pipelines for human MRIs, but very few automated methods for extraction of cortical surfaces have been reported for NHPs and none have been tested on data from diverse sources. We present PREEMACS, a pipeline that standardizes the preprocessing of structural MRI images (T1- and T2-weighted) and carries out an automatic surface extraction of the macaque brain. Building upon and extending pre-existing tools, the first module performs volume orientation, image cropping, intensity non-uniformity correction, and volume averaging, before skull-stripping through a convolutional neural network. The second module performs quality control using an adaptation of MRIqc method to extract objective quality metrics that are then used to determine the likelihood of accurate brain surface estimation. The third and final module estimates the white matter (wm) and pial surfaces from the T1-weighted volume (T1w) using an NHP customized version of FreeSurfer aided by the T2-weighted volumes (T2w). To evaluate the generalizability of PREEMACS, we tested the pipeline using 57 T1w/T2w NHP volumes acquired at 11 different sites from the PRIME-DE public dataset. Results showed an accurate and robust automatic brain surface extraction from images that passed the quality control segment of our pipeline. This work offers a robust, efficient and generalizable pipeline for the automatic standardization of MRI surface analysis on NHP.

I. Introduction

Research about brain structure and function in non-human primates (NHPs) is fundamental to understand both the neural substrate of human cognition and the sources of brain dysfunction in different neurological populations (Mendoza and Merchant, 2014; Merchant et al., 2015; Buffalo et al., 2019). Important recent progress on multimodal and multi-scale neuroimaging technologies in NHPs have opened a window to investigate many critical structural-functional properties of the brain (Milham et al., 2020); these include the study of structural brain changes during development, aging, and models of neurological disorders (Goldberg, 2019).

With the objective of accelerating the research in NHP and promote collaboration, a recent worldwide initiative, the Primate Data Exchange or PRIME-DE, has been created for data sharing and the development

of open resources for NHP imaging (Milham et al., 2018, 2020). Nevertheless, a major obstacle for the community is the lack of fully validated pipelines and automated methods for data preprocessing and surface extraction of macaque MRI structural data. Consequently, in this paper we describe PREEMACS, a pipeline that standardizes the preprocessing of raw structural MRI images (T1- and T2-weighted) for the extraction of cortical surfaces in macaque NHPs with minimal or no manual intervention.

1.1. Why study the cortical surface in NHP?

For the last 20 years, the use of MRI surface-based methods has been a crucial tool to study the human cortical structure. These methods include several cortical morphometric measures such as cortical thickness (CT), cortical surface area (SA), and gyrification (Lerch et al. 2017). CT

P. Garcia-Saldivar, A. Garimella, E.A. Garza-Villarreal et al.

NeuroImage 227 (2021) 117671

is a macroscopic parameter that provides relevant information about atrophy, as well as cortical plasticity (Scholtens et al., 2015). The morphology of the brain surface is regarded as an important endophenotype in neurological and psychiatric disorders (Davatzikos et al., 2011; MRC AIMS Consortium et al., 2019; Whelan et al., 2018). Neurodevelopmental studies have reported changes of CT and SA at different ages, which relate to age-specific neuronal pruning, myelin concentration, and cortical reorganization (Zhou et al., 2013; Li et al., 2015; Shaw et al., 2008; Wierenga et al., 2014). In addition, measures like CT are sensitive to cortical changes in myelin and cytoarchitecture within days and weeks, enabling studies of task-related cortical plasticity (Sampaio-Baptista and Johansen-Berg, 2017). Thus, the quantitative assessment of changes of cortical morphometry using MRI surface-based methods is a powerful non-invasive technique to investigate brain structure in many areas of neuroscience research. Notably, using MRI in NHPs as a model for brain plasticity, development and neurological diseases provides essential benefits over human MRI datasets (Van Essen and Dierker, 2007). First, scanning NHPs under highly controlled anesthesia protocols permits acquisition of virtually motion-free images with high quality and resolution, with the added benefit of longer scan times than those feasible in human subjects (Milham et al., 2020). Second, while recruiting and following a homogeneous group of subjects to track individual MRI changes over time remains a large problem in human studies, NHP studies allow for great control in longitudinal studies and are better suited to isolate the effects of experimental interventions (Scott et al., 2016; Song et al., this issue) and the reconfiguration of the cortical sheet after intensive training in complex cognitive tasks (Fortes et al., 2004; Crowe et al., 2014; Merchant and Averbeck, 2017). Finally, NHP structural MRIs can be combined with invasive experimental conditions that are impossible to implement in human studies, such as pharmacological interventions (Yc et al., 2019), histological studies (Sultan et al., 2010; Naselaris et al., 2005; Georgopoulos et al., 2007; Caminiti et al., 2009), and high density electrophysiological recordings (Schwartz et al., 2014; Mendoza et al., 2016), as well as the injection of viral vectors for optogenetic manipulations (Galvan et al., 2017) or Calcium imaging (Li et al., 2017), which provides a unique way to understand the human brain and its pathologies. Therefore, the use of these combined methodologies can shed light on fundamental information about the molecular, structural and brain circuit mechanisms behind changes in cortical thickness associated with development, learning, and neurological and psychiatric disorders (Buffalo et al., 2019).

Despite their aforementioned advantages, surface-based methods have been scantly used in NHPs and confront the following technical issues: 1) the inability of specialized software to natively support submillimetric resolution NHP brain volumes, 2) lack of precise brain extraction algorithms adapted specifically for macaques, 3) the heterogeneity of MRI acquisition methods, and 4) a lack of consensus on image preprocessing (Gronenschild et al., 2012). PREEMACS provides a unified analytical framework that solves these issues and generalizes across different image acquisition schemes and research institutions around the world.

1.2. The value of accurate cortical surface estimations

Determination of the pial (outer) and white matter (inner, i.e., the boundary between the cortex and underlying white matter) surfaces is central to accurate CT estimation. Errors in the estimations of these surfaces produce artificially higher or lower CT that potentially affect the results (Ducharme et al., 2016; Rosen et al., 2018). Partial volume effects (PVE) due to MRI resolution is a common problem in MRI that can blur the boundaries of gyri and sulci difficulting their identification (Rueda et al., 2010). For this reason, correct data acquisition, data preprocessing and quality control are of the highest priority. Proper segmentation of gray and white matter, as well as CSF, are critical for surfaces reconstruction (Eggert et al., 2012). Moreover, multiple algorithms exist that calculate and determine the outer- and inner-surface bound-

aries, such as: "Marching Cubes", a bottom-up method using edge detection used in CIVET (Kim et al., 2005), SureFit in Caret (Zhong et al., 2010), volumetric-based method in ANTs (Tustison et al., 2014), and Bayesian approaches (Miller et al., 2000). All algorithms and methods are prone to errors and inaccuracies that need to be addressed and minimized when conducting surface estimations (Zhong et al., 2010). Notably, these methods have mostly been optimized for human brain imaging and they application to NHPs has been proved challenging. Indeed, this situation has led to each research group developing site-specific adaptations of existing tools, with poor generalization, or developing new methods from the ground up (Oguz et al., 2015).

1.3. The importance of quality control in NHP MRI

Results from image processing pipeline can only be as good as the raw data will allow. Quality assurance is, therefore, an obligatory first step. Semi-automated quality control (QC) has gained traction due to the ever-increasing generation of large amounts of imaging data (big data) in MRI, with datasets prohibitively large to curate manually (Alfaro-Almagro et al., 2018; Klapwijk et al., 2019). Recent efforts in QC for big data analysis demonstrate that curation is a necessity to reduce variability and increase statistical power in morphological data (MRC AIMS Consortium et al., 2019). Automated extraction of QC metrics and their intuitive visualization has been adopted by recent software such as MRIqc (Esteban et al., 2017), which provides an easy to use HTML-based interface to quickly curate human neuroimaging data. The importance of QC is accentuated with NHP MRI data where there is increased variability due to the type of image sequences used, as well as their orientation, geometry, and other parameters (Milham et al., 2018). The present pipeline relies on different MRIqc-based metrics to determine whether the input NHP images are of enough quality to produce adequate estimates of brain surfaces and CT measurements.

Here, we aimed at developing a robust, automatic and versatile preprocessing pipeline for macaque cortical surface estimation. Our workflow deals with many specific challenges of the NHP structural images and was validated on 57 images from 11 different sites from the PRIME-DE. Specifically, PREEMACS carries out automatic skull striping, performs a quality control assessment on input images that predicts the quality of the surface outcome, uses three custom made macaque templates for surface segmentation and registration within the pipeline, keeps all images and the resulting surfaces in native space, and runs all the steps automatically within the workflow until the CT group data analysis.

2. Material and methods

2.1. UNAM-INB dataset

2.1.1. Subjects

Eight rhesus monkeys (*Macaca mulatta*, six males, 4–10 years old, weight 5–12 kg) were scanned under anesthesia. Animal care, housing, and experimental procedures were approved by the National Autonomous University of Mexico Institutional Animal Care and Use Committee (protocol 090.A INB) following the principles outlined in the Guide for Care and Use of Laboratory Animals (NIH, publication number 85–23, revised 1985).

2.1.2. Data acquisition

Anesthesia

Anesthesia was induced with an initial dose of ketamine/xylazine (IM 7/0.6 mg per Kg) and maintained with additional doses of ketamine/xylazine (IM 2.5/0.05 mg per Kg) every 30 min. Animals were monitored continuously with a pulse oximeter to track heart rate and peripheral capillary oxygen saturation.

Imaging protocol

Images were acquired using a 3 T Philips Achieva TX scanner with a 32-channel head coil for humans. Animals were placed inside the scanner in an inverted sphinx position, which minimizes the distance between the animal's head and the coil and improves signal-to-noise ratio (SNR). A vitamin E capsule affixed to the right portion of the head to unequivocally ascertain left/right hemispheres throughout subsequent image processing steps. In order to ensure the same position of all animals in the scanner, based on https://caseforge.co models, we used a custom-made plastic helmet specifically designed for the 32-channel head coil with removable tailor-made padding adapted to each monkey's head. These precautions minimized motion and avoided direct contact of the monkey's head with the coil. T1w volumes were acquired using a spoiled gradient echo sequence using three-dimensional spatial encoding, with slices collected in the sagittal plane (frequency encoding = anterior/posterior), with imaging parameters as follows: TR/TE=3.1/5.24 ms, flip angle = 8°, SENSE, field of view (FOV) = $128 \times 128 \times 145$ mm^3, matrix size = $184 \times 143 \times 183$ slices, yielding voxel resolution = $0.7 \times 0.5 \times 0.5$ mm^3. We obtained 6 T1w images per animal. Four T2w volumes in the sagittal plane (frequency encoding = anterior/posterior) were acquired using a turbo spin echo sequence with three-dimensional spatial encoding, with an isometric voxel resolution of 0.5 mm, matrix size= $256 \times 256 \times 290$ slices, SENSE, TR/TE=2500/338 ms, flip angle = 90°, FOV=$256 \times 256 \times 100$ mm^3. The manufacturer's default surface coil intensity (SCIC) filter was applied to all images prior to further processing.

2.2. PREEMACS modules

PREEMACS has a modular design, with each module running independently. These modules perform the canonical workflow for pre-processing MRI (Glasser et al., 2013; Alfaro-Almagro et al., 2018; Esteban, et al., 2019), except for the steps that are specific for NHP data using different previously-available functions from FSL (FM-RIB's Software Library – FSL, Oxford, U.K) (Smith et al., 2004), ANTs (Avants et al., 2011), MRtrix (Tournier et al., 2019), MRIqc (Esteban et al., 2017) and FreeSurfer (Dale et al., 1999; Fischl et al., 1999b; Fischl, 2012). Inputs to the pipeline are one (or more) T1w volumes and one (or more) T2w volumes per animal (Fig. 1A).

2.2.1. Module 1: preprocessing

This module prepares the raw images (T1w and T2w) for initial processing and is constituted by the following six steps (Fig. 1B):

Volume orientation: Since brain images of the NHP can be acquired with the subjects in different positions (e.g. lateral, sphinx, supine) within the scanner, it is necessary to reorient the image. This step generates an output volume in RAS space relative to the sphinx position (Right->left; Anterior->posterior; Superior->inferior).

Image crop. The FOV of NHP MRI acquisition often includes anatomy beyond the head of the animal. This extra information can increase between-subject variance and make spatial normalization difficult. Therefore, PREEMACS crops the brain and parts of the skull automatically in native space. This crop is performed using a mask whose geometry depends on the coordinates of the anterior and posterior commissures. These coordinates are estimated by aligning the T1w volume to the NMT template (Seidlitz et al., 2018) through a linear registration with 6 degrees of freedom (DOF) using ANTs (Avants et al., 2011), then back to native space. If registration fails, then PREEMACS asks the user to provide the coordinates of anterior and posterior commissures to crop the images.

Intensity non-uniformity (INU) correction: Most NHP images contain spatially varying intensity non-uniformities. Common sources of non-uniformities include the use of multi-channel coils, the position of the animal with respect to the coil, and B1 inhomogeneities. Image segmentation, in turn, is likely to fail unless these non-uniformities are properly corrected. Intensity normalization is performed with the N4 algorithm (Tustison et al., 2010) on every volume, prior to averaging. For improving the performance of the N4 algorithm the b-spline fitting parameter was tuned empirically (-b [100 mm]).

Image averaging, resampling and conform: The T1w and T2w volumes are averaged separately for each contrast. This is performed using the tool mri_motion_correct.fsl of FreeSurfer. Each of the two resulting volumes are resampled to obtain an isometric resolution of 0.5 mm and a final size of $256 \times 256 \times 256$ voxels.

Skull-stripping: Obtaining an accurate mask of the brain is a crucial step for image processing. While there are many tools for skull-stripping in human MRI (Kleesiek et al., 2016; (Eskildsen et al., 2012; Iglesias et al., 2011; Smith, 2002), we encounter far fewer tools for NHP, including: Marker based watershed scalper (MBWSS) (Beare et al., 2013), 3dSkullStrip of AFNI (Cox, 1996), Primatologist-Toolbox (Balbastre et al., 2017), NMT_subject_align.sh (Seidlitz et al., 2018), and automated template derived brain extraction in animal MRI (atlasBREX) (Lohmeier et al., 2019). Nevertheless, the brain segmentation obtained using these tools, in most cases, shows estimation errors in the prefrontal cortex and the temporal lobes, as well as errors in the separation of the dura and gray matter. To solve this problem, we customized the Python module DeepBrain (Itzcovich, 2017), which was designed for skull-stripping in human MRI using a convolutional neural network implemented on Tensorflow, to work with NHP data. We trained the DeepBrain model using a set of T1w monkey images and the corresponding manually-defined brain masks. Notably, the data augmentation strategy implemented in DeepBrain increases the variability of image orientation in order to obtain a richer input dataset. We refer to this skull striping method based on the convolutional neural network model as the PREEMACS brainmask tool. The preprocessing of the images for training the convolutional neural network was the following: First, we executed the first module of PREEMACS through step "*Image averaging, resampling and conform*" using a total of 126 images: 88 images from PRIME-DE (sampling at least an image per PRIME-DE site from 17 sites), 17 from UNAM-INB, and 21 from UNC-Wisconsin dataset (Young et al., 2017). Second, we built a brain mask for each image as follows. For the PRIME-DE and UNAM-INB datasets, we built the brain masks using the atlasBREX pipeline and performed the corresponding manual correction. The masks included all cerebral and cerebellar gray matter and white matter, as well as the brainstem (pons, medulla). Skull, skin, muscles, fat, eyes, dura mater, bone and the optic chiasm were excluded from the mask. In the case of the UNC-Wisconsin dataset, manual segmentation of the images was already available, so we only excluded the optic chiasm from the original masks.

The degree of overlap between the mask computed with the PREEMACS brainmask tool and the manually drawn reference mask was determined using three metrics: Dice coefficient (Dice, 1945), Sensitivity and Specificity (Kleesiek et al., 2016). These measures depend on the following four parameters: false negatives (FNs) defined as voxels that are removed by the Deep Neural Network method but are present in the reference mask; false positives (FPs), defined as voxels which have been predicted incorrectly as brain tissue; true positives (TP), that correspond to the voxels that were correctly identified by the PREEMACS brainmask tool as brain tissue; and true negatives (TN), defined as the voxels correctly identified as non-brain tissue. Dice is the most commonly used coefficient to compare two segmentations (Kleesiek et al., 2016; Manjon et al., 2014; Wang et al., 2014) and is defined as the ratio of twice the size of the intersection of the two masks relative to the sum of their sizes, as follows:

$$\text{Dice} = \frac{2TP}{2TP + FP + FN}$$

Based on Kleesiek et al. (2016), we also computed the sensitivity (TP/(TP+FN)) and specificity (TN/(TN+FP)) scores.

2.2.2. Module 2: quality control

Since images with acquisition artifacts could induce biases and segmentation miscalculations, a rigorous quality control of the input im-
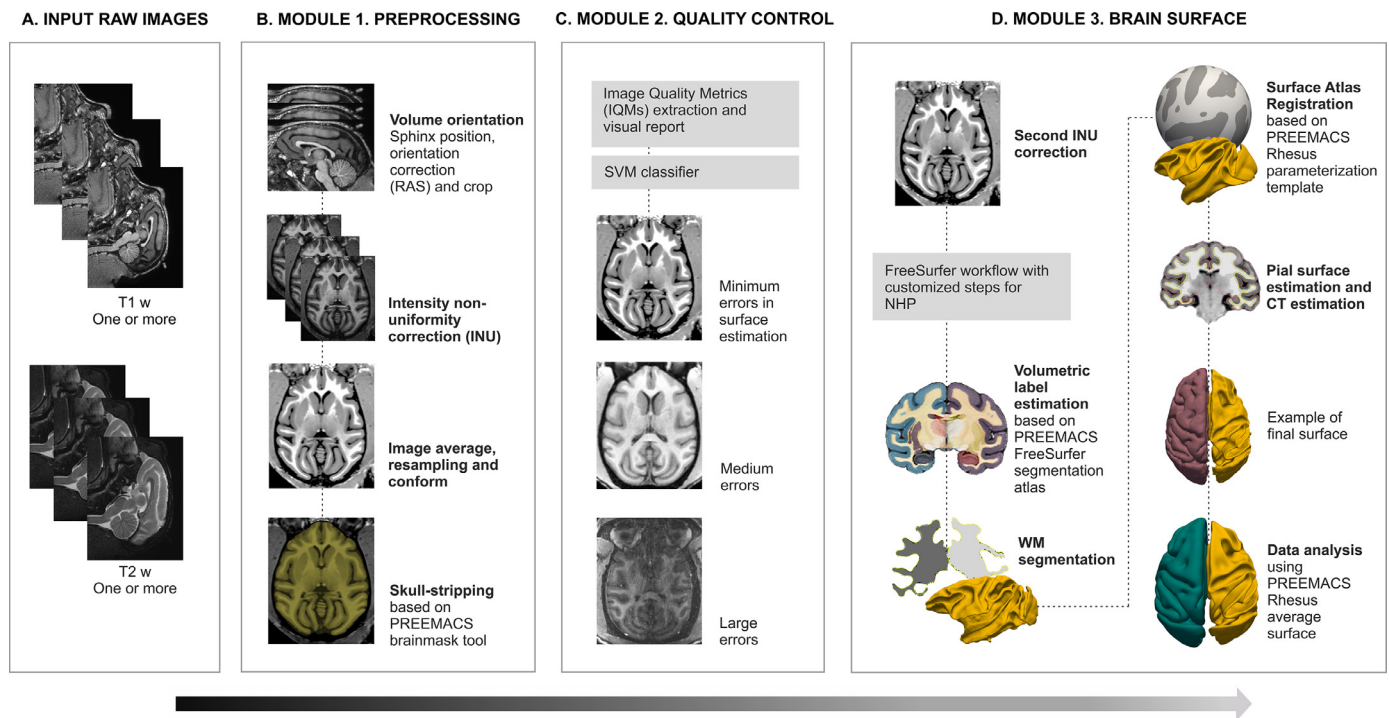
Fig. 1. Pipeline for PREprocessing and Extraction of the MACaque brain Surface (PREEMACS). A. Input raw images. B. Module 1 performs volume orientation, image cropping, INU correction, image average, and skull-stripping. C. Module 2 performs quality control using an adaptation of the MRIqc method and extracts quantitative quality metrics, which are used to determine the likelihood of a successful brain extraction based on a SVM classifier. D. Module 3 estimates the white matter (WM) and pial surfaces from T1w using an NHP customized version of FreeSurfer 6.0. After a second INU correction, a volumetric label estimation is carried out based on our PREEMACS FreeSurfer segmentation atlas. Then, WM segmentation is performed and the WM surface is registered to the PREEMACS Rhesus parameterization template. The pial surface is properly estimated with the help of the T2w image. Finally, CT is calculated and the resulting surfaces can be analyzed in the geometric space of PREEMACS Rhesus average surface.

ages is of utmost importance for the automatic identification of cortical surfaces. Here, we adapted the structural MRI Quality Control tool MRIqc v0.15.2 (Esteban et al., 2017) to work with NHPs. Specifically, we performed the following adaptations to MRIqc for monkey images: conform, skull-stripping, spatial normalization to the NMT monkey template (Seidlitz et al., 2018) space with a high-resolution template ($0.25 \times 0.25 \times 0.25$ mm^3), and replacement of all human template images (brain template, brain mask, head mask and probabilistic segmentation files) with the NMT template. As a result of these modifications, the MRIqc pipeline is fully compatible with NHP images. MRIqc carries out the brain segmentation and estimates the brain masks to finally compute the image quality metrics (IQMs). From the total 68 metrics calculated by MRIqc, we used 58 for further analysis. The other ten metrics were excluded because they related to voxel and FOV sizes, which are constant across the resampled images, measure background artifacts of parts of the images that PREEMACS crops or could not be reliably computed across images. In addition, six structural datasets were not included since their signal-to-noise ratio was very low and did not allow for the computation of IQMs.

PREEMACS uses these IQMs as predictors of the quality of the resulting surface using a Support Vector Machine (SVM), where the three possible outcomes of the classifier are surfaces with minimum, medium or large errors (Fig. 1C). The SVM was trained one hundred times with a twenty-fold cross-validation to evaluate the performance of the classifier. The training dataset of the SVM were the 58 IQMs of 57 T1 images (52 MRIs from PRIME-DE and 5 MRIs from UNAM-INB) and for which the target class (minimum, medium or large errors) was defined using a visual inspection test on the wm/gm PREEMACS surfaces. This test uses a rating scale between 0 and 48 points depending on the smoothness of the surfaces and presence of segmentation errors. The smoothness takes values between 0 for perfectly smooth and 10 for very irregular surfaces.

The segmentation rating can acquire values between 0 for no errors and 38 for widespread errors in the wm across all cortical areas. The values of the visual inspection test were ranked as minimal for 0–9, medium for 10–15, and larger errors for 16–48. Surfaces with large errors on the visual inspection test would require major manual intervention.

We investigated whether some metrics contained more information to predict the quality of the obtained surfaces. To this end, we computed a dissimilarity matrix for all possible metrics pairs using the Calinski–Harabasz index as a distance measure (Calinski and Harabasz, 1974). This index measures the clustering power of a metric pair to separate the three outcome surfaces and corresponds to the ratio of the intra- to the inter-cluster dispersion with larger scores for better clustering. This matrix was treated as the adjacency matrix for a weighted undirected graph. The threshold was found through an edge density minimization approach, whereby the graph density (K), defined as $K = n / (N \times (N-1))$, where n is the number of edges in the graph and N the total number of metrics, was iteratively calculated for an increasing threshold, starting at zero and reaching the maximum Calinski–Harabasz index in the matrix, progressively eliminating edges that did not reach each threshold and nodes that lost all its edges.

Therefore, the threshold to extract the final graph is the index that minimized the edge density, because at this point the graph conveys the maximal information about its complex topology (Royer et al., 2008). As depicted in Fig. 3A, the threshold had a Calinski–Harabasz index of 14.7 and the edge density at the threshold was 0.08.

2.2.3. Module 3: brain surface estimation

The purpose of this module is to obtain the CT of the brain surface using a customized version of FreeSurfer v6 optimized for NHP images (Fig. 1D). This module uses the skull-stripped images obtained

P. Garcia-Saldivar, A. Garimella, E.A. Garza-Villarreal et al.

NeuroImage 227 (2021) 117671

Table 1
Adaptations of FreeSurfer recon-all pipeline.

FreeSurfer Flag	Step	Status
autorecon1	Motion correction and conform	FreeSurfer v.6
	Non-uniform intensity normalization	FreeSurfer v.6
	Talairach transform conformation	PREEMACS customized
	Intensity normalization I	FreeSurfer v.6
	Skull stripping	replaced by PREEMACS brain mask tool
autorecon2	Linear volumetric registration to Gaussian Classifier Atlas (GCA)	FreeSurfer v.6
	Intensity Normalization based on GCA model	FreeSurfer v.6
	Non-linear volumetric registration to GCA atlas	FreeSurfer v.6
	Remove neck	Deleted
	Align volume with skull to GCA atlas	FreeSurfer v.6
	Volumetric labeling estimation	PREEMACS customized
	Intensity normalization 2	PREEMACS customized
	WM segmentation	PREEMACS customized
	Edit WM with volumetric labeling	PREEMACS customized
	Fill	FreeSurfer v.6
	Tessellation	FreeSurfer v.6
	Smooth 1	FreeSurfer v.6
	Inflate 1	FreeSurfer v.6
	Qsphere	FreeSurfer v.6
	Automatic topology fixer	FreeSurfer v.6
autorecon3	Final surfaces	PREEMACS customized
	Smooth 2	FreeSurfer v.6
	Inflate 2	FreeSurfer v.6
	Spherical mapping	PREEMACS customized
	Spherical registration	PREEMACS customized
	Spherical registration, contralateral hemisphere	PREEMACS customized
	Cortical ribbon mask	FreeSurfer v.6

from Module 1. Output surfaces are provided in Freesurfer and GIFTI formats.

Second INU correction: Certain averaged volumes can have persisting image intensity non-uniformities (INU). PREEMACS uses the BiasFieldCorrection_sqrtT1wXT1w.sh pipeline from HCP to address this issue (Glasser et al., 2013) based on procedures described in Rilling et al. (2012). Briefly, the T2w image is aligned to the T1w image with a 6 DOF rigid-body transformation using ANTs tool, then the bias field is estimated and corrected for based on the square root of T1w × T2w.

Voxel image size: Most of Freesurfer's tools expect images to be conformed to an isometric resolution of 1 mm per side, and to have a specific FOV of 256 voxels per side. Given that NHP volumes typically have submillimeter resolution not accepted by most software, the image header is edited to fake isometric resolution of 1 mm (yet the image data is not resampled) (Donahue et al., 2016).

FreeSurfer processing: FreeSurfer is a suite of tools for the analysis of neuroimaging data using automated workflows to quantify structural properties of the human brain based on surface measures (Fischl, 2012). Freesurfer's main pipeline for human brain surface extraction is called recon-all, which is in turn divided into three parts denominated autorecon 1, 2, and 3. Specific adaptations of recon-all have been made in PREEMACS to work with NHP images, which are outlined in Table 1.

Modifications in Autorecon 1. For this part of the pipeline we developed two adaptations. Firstly, multiple steps of the FreeSurfer workflow required the use of talairach coordinates as seed points. To obtain these coordinates, FreeSurfer performs an affine registration (Dale et al., 1999) to the MNI305 atlas, using 4dfp image registration tools distributed as a part FreeSurfer, and keeps the transformation matrix as an .xfm file. Our pipeline uses a Rhesus template image in MNI space (namely the NMT template) instead of freesurfer's default MNI305 tem-

plate. The second adaptation is the use of our skull-stripping procedure based on a convolutional neural network, as described previously (Section "*Skull-stripping*").

Modifications in Autorecon2

Volumetric label estimation. To improve the wm/gm segmentation, it is necessary to perform brain structural parcellation based on an atlas. For each subject, FreeSurfer obtains the cortical and subcortical structure labels by non-linear registration using the Gaussian Classifier Atlas (GCA) (Fischl et al., 2002). This human-based parcellation is used in different steps throughout Freesurfer's workflow such as wm segmentation, segmentation of the cerebellum and pons among others. We replaced the GCA with a custom NHP segmentation (PREEMACS FreeSurfer segmentation atlas, see below for details). Label estimation for each subject is obtained by registering the generic NMT atlas, a space where the PREEMACS FreeSurfer segmentation atlas was designed, to the corresponding T1w using a non-linear transformation (diffeomorphic) registration using ANTs (Avants et al., 2012).

White matter segmentation. Two adaptations were developed in PREEMACS to obtain a robust wm segmentation. First, the wm was segmented using a wm mask (Dale et al., 1999). This wm mask includes empty spaces on subcortical gm in the human FreeSurfer workflow. These spaces are filled using a subcortical mask. To solve this issue in NHP, the subcortical structures are identified using our PREEMACS FreeSurfer segmentation atlas. Then, the identified areas are filled as wm in the mask.

Second, we customized the FreeSurfer pipeline to minimize a common segmentation error in NHP MRIs consisting of a strong intensity bias with high intensity values in the precentral gyrus and the visual cortex. The problem was solved using the High Intensity Control Point (HICPO) tool, developed and implemented in our workflow. The HICPO estimates the WM in the precentral gyrus (PCg) and in the visual cortex using a higher (stricter) volume segmentation threshold and a normal threshold over the rest of the cortex. We follow the standard FreeSurfer process for the wm segmentation using the mri_segment tool for both thresholds. Then, we created a mask on the high thresholded areas and used it to replace the precentral gyrus and the visual cortex on the brain volume with low threshold segmentation.

Modifications in Autorecon3

Surface atlas registration. Since the number of vertices is not the same among the subjects and depends on the brain size of each monkey, the wm surface in native space needs to be registered to a common space (Fischl et al., 1999a, 1999b). This step computes a subject's sphere from the wm inflated surface, warps the sphere into a 2-D file containing the curvature and convexity pattern of the subject, and then registers the 2D file with a reference pattern called PREEMACS Rhesus parameterization template (detailed below). This is executed to ensure that the monkey´s curvature and convexity pattern are aligned with a generic Rhesus NHP reference template. Thus, these metrics allow us to establish a surface-based coordinate system (Fischl et al., 1999a) with vertex correspondence between subjects, such that anatomical features can be compared between animals for group analysis. For registration, FreeSurfer uses mris_register, which represents deformation by a displacement field on the sphere. This algorithm minimizes areal distortions, so that the overall change in area of triangular mesh faces during the transformation is minimized (Fischl et al., 1999a). After that, the pial surface is created by expanding the white matter surface so that it closely follows the gray-CSF intensity gradient, keeping the same topology (number of vertices, edges, faces). During inflation, indexed vertices in each surface space retain one-to-one correspondence, such that each index represents the same cortical location across white, pial, inflated and spherical surfaces. Due to the surfaces are not matched across hemispheres within individuals, the data associated with each vertex are sampled into the group space in order to obtain vertex correspondence across subjects.

Pial surface and cortical thickness estimation. Final estimation of the pial surface is estimated using T2w images. In order to improve pial estimation we carried out three modifications on the FreeSurfer pipeline

P. Garcia-Saldivar, A. Garimella, E.A. Garza-Villarreal et al.

NeuroImage 227 (2021) 117671

(Supplementary Figs. 1 and 2) (Fischl et al., 1999a). The first modification corrects the commonly observed intersection in pial surfaces between hemispheres. We initially estimate the difference between the cortical ribbon from T1w and T2w images. Then, the correction is carried out by subtracting this ribbon difference from the T2w images, focusing on an ROI that is made of two sagittal slices of the intermediate wall. Second, to avoid segmentation errors from the hippocampus and amygdala, we used our atlas to identify and eliminate these structures from the final images. Finally, PREEMACS estimates the cortical thickness modifying the maximum cortical thickness parameter (from the default 5 mm to 10 mm) to ensure that the fake 1 mm space (see *Voxel image size*) does not set a low cap on cortical thickness (Donahue et al., 2018).

Template building: Three NHPs templates were built within the FreeSurfer environment: (1) PREEMACS FreeSurfer segmentation atlas, with cortical and subcortical labels, (2) PREEMACS Rhesus parameterization template, that includes the Rhesus curvature and sulcal pattern templates for individual monkey wm surface registration, (3) PREEMACS Rhesus average surface for final mapping of vertices across all animals. The last two templates were constructed using 33 monkey MRIs from the (29 MRIs) PRIME-DE and (4 MRIs) UNAM-INB datasets.

PREEMACS FreeSurfer segmentation atlas: We created an atlas with FreeSurfer format labels in NMT space. This atlas was built using the D99 template segmentation and registered to the NMT space, using a non-rigid transformation (diffeomorphic) using ANTs (Avants et al., 2012). The segmentation was corrected manually, and hippocampus, thalamus, claustrum, ventral diencephalon, brainstem, and corpus callosum were manually added.

PREEMACS Rhesus parameterization template: First, each T1 image was linearly registered (6 dof) to the NMT space. Second, with these registered images we executed the PREEMACS workflow until the sphere creation step, where we obtained the wm sphere surface from both hemispheres. Next, we created a parameterization file (PREEMACS Rhesus parameterization file) following the steps described in the FreeSurfer wiki http://surfer.nmr.mgh.harvard.edu/fswiki/SurfaceRegAndTemplates creating a registration template across all animals (Fischl et al., 1999b). A FreeSurfer workflow was designed to build, for each hemisphere, a parameterization template file in 2D TIFF format. This parameterization file contains nine elements with information about the mean and variance (across subjects) of the curvature pattern (estimated from both the smooth and inflated wm surface), the mean and variance of the convexity pattern (using the smooth wm surface), and the degrees of freedom (number of subjects) used for the statistic calculation of the three patterns. The variance is used to lower the weights of features with high fluctuations across subjects, so that the registration depends on the stable features like the curvature and convexity patterns of the central/calcarine/sylvian sulci in the inflated surface. The parameterization template file was built by adding subjects iteratively, initializing the process with the information of the NMT wm surface to avoid biasing the estimation.

PREEMACS Rhesus average surface: In order to obtain a template for the geometric representation of the wm and pial surfaces, we created an average surfaces using the steps described in the FreeSurfer wiki http://surfer.nmr.mgh.harvard.edu/fswiki/SurfaceRegAndTemplates. The vertex correspondence across subjects is computed only for group analysis, so the subjects´ overlays (e.g. thickness) are sampled into the group space (not the surface geometries themselves).

3. Results

To evaluate the generalizability of our method, we tested the PREEMACS workflow with the PRIME-DE (Milham et al., 2018) data set. The PRIME-DE is an open source dataset with 217 NHP subjects from twenty-seven different sites. This database contains T1w, T2w, fMRI and DWI scans. These images were acquired with different scanners, coils, structural MRI protocols and macaque species (*Macaca mulatta and Macaca*

Table 2
Number of images used across the different modules for the development and validation of PREEMACS.

Process	Number of subjects	Database
Assessment of the generalizability of PREEMACS pipeline	52	PRIME-DE
PREEMACS Rhesus average surfaces	33	PRIME-DE and UNAM-INB
PREEMACS brainmask tool	126	PRIME-DE, UNAM-INB, UNC- WISCONSIN
MRIqc classifier model	57	PRIME-DE, UNAM-INB
PREEMACS pipeline development	5	UNAM-INB

fascicularis). Consequently, we only selected images that met the following criteria: MRIs with both T1w and T2w sequences, available to download online (without special requirements), no cropping or masks, and only one set of images per animal. In addition, phase-sensitive inversion recovery (e.g. Real-IR) images were eliminated as FreeSurfer produces errors in the tissue classification step. Fifty-eight images from PRIME-DE plus five images from our UNAM-INB database met these requirements. Nevertheless, we excluded six subjects due to their low signal-to-noise ratio. Thus, a total of fifty-seven monkey images from eleven sites across the world were used to evaluate all modules of PREEMACS. See Table 2 for a detailed description of the number of images used across the different modules of PREEMACS.

3.1. PREEMACS brainmask tool

We developed a skull stripping method based on a deep learning algorithm that obtains accurate brain masks solving one of the most common bottlenecks in surface-based estimations. Fig. 2A shows values of Dice, Sensitivity and Specificity for 126 masks obtained with PREEMACS brainmask tool. These metrics were designed to measure the overlap between the computed against the manually drawn mask, with values between zero (no overlap) and one (perfect overlap) (see Materials and Methods). The results showed values close to one for the three metrics across sites with a mean ($\pm$SEM) for Dice of 0.97 ± 0.009, Sensitivity of 0.96 ± 0.01, and Specificity of 0.99 ± 0.0006, supporting the notion that our Deep Neural Network implementation for skull stripping was very robust across a wide variety of images and sites. Nevertheless, the sensitivity showed values between 1 and 0.9, indicating some degree of false negative rate, and hence, that the predicted masks were smaller than the reference. This can be explained by the tendency to overestimate a manually drawn mask. In contrast, the false positives were very scarce since the specificity was very close to one. Indeed, Fig. 2B illustrates the clear segmentation of five brain masks computed from images collected from different sites.

3.3. Surface quality prediction based on IQMs

Using 58 IQMs we trained SVMs to classify volumetric structural images that produced 57 PREEMACS surfaces into groups with minimum, medium, and large errors. We used visual scoring (see methods for details) on the properties of the volumetric structural images in order to predict with SVMs the quality/reliability of the output surfaces. The classifier performance showed 66 ± 1.9 (mean $\pm$ STD) percent of correct predictions, considerably higher than chance (33.3%, for 3 classes). However, we hypothesized that not all metrics contain useful information to predict the quality of the obtained surfaces. Therefore, we selected those metrics that maximized the classification based on graph analysis (see Section 2.2.2). Notably, five IQMs showed large clustering power to distinguish between outcome surface categories (Fig. 3B), forming a maximum clique with a high degree of centrality (Fig. 3C,D).
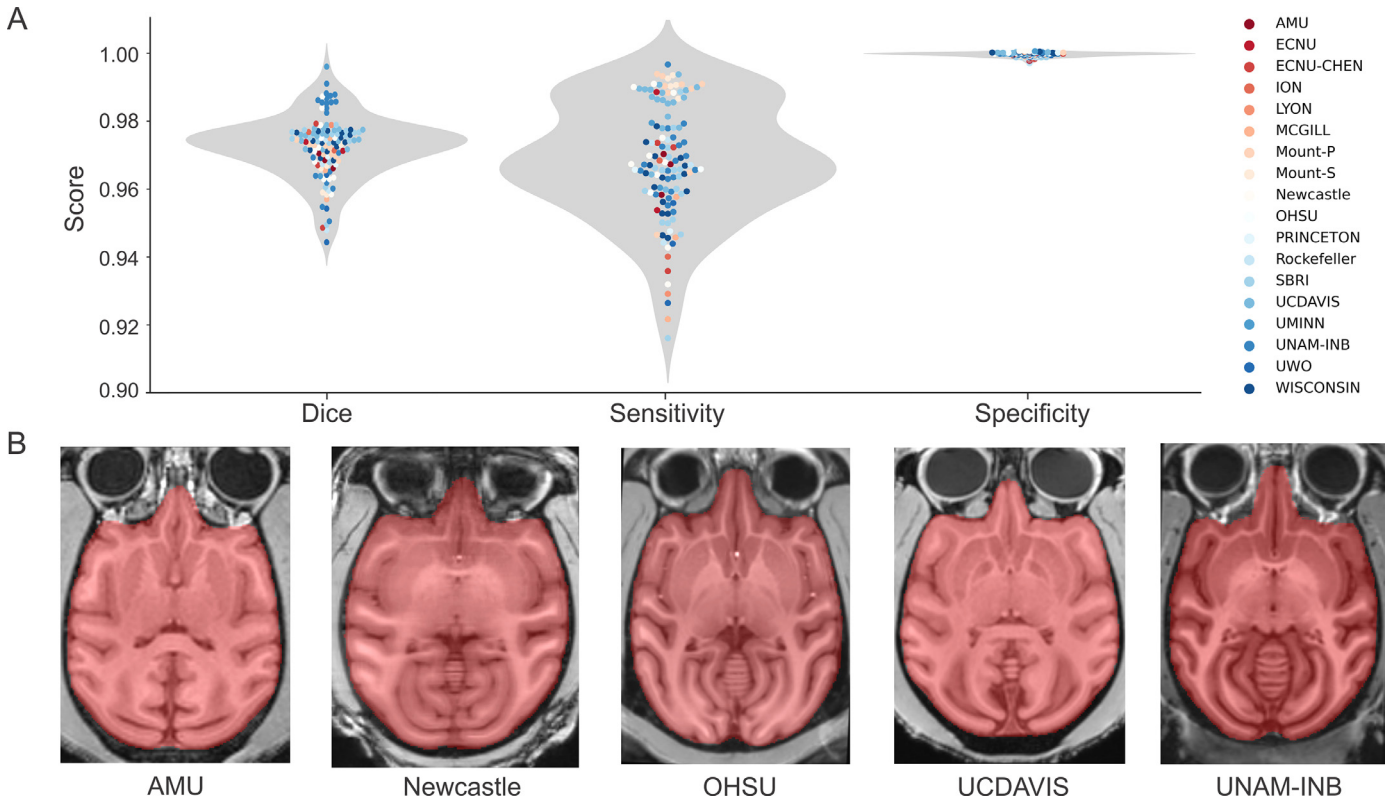
Fig. 2. Performance of the PREEMACS brainmask tool that uses a Deep Learning convolutional neural network model. A. The violin plots for the Dice, Sensitivity and Specificity metrics computed across 18 sites (color coded, see inset) for 126 monkey images. B. Brain masks (red) for five monkeys of different provenance.
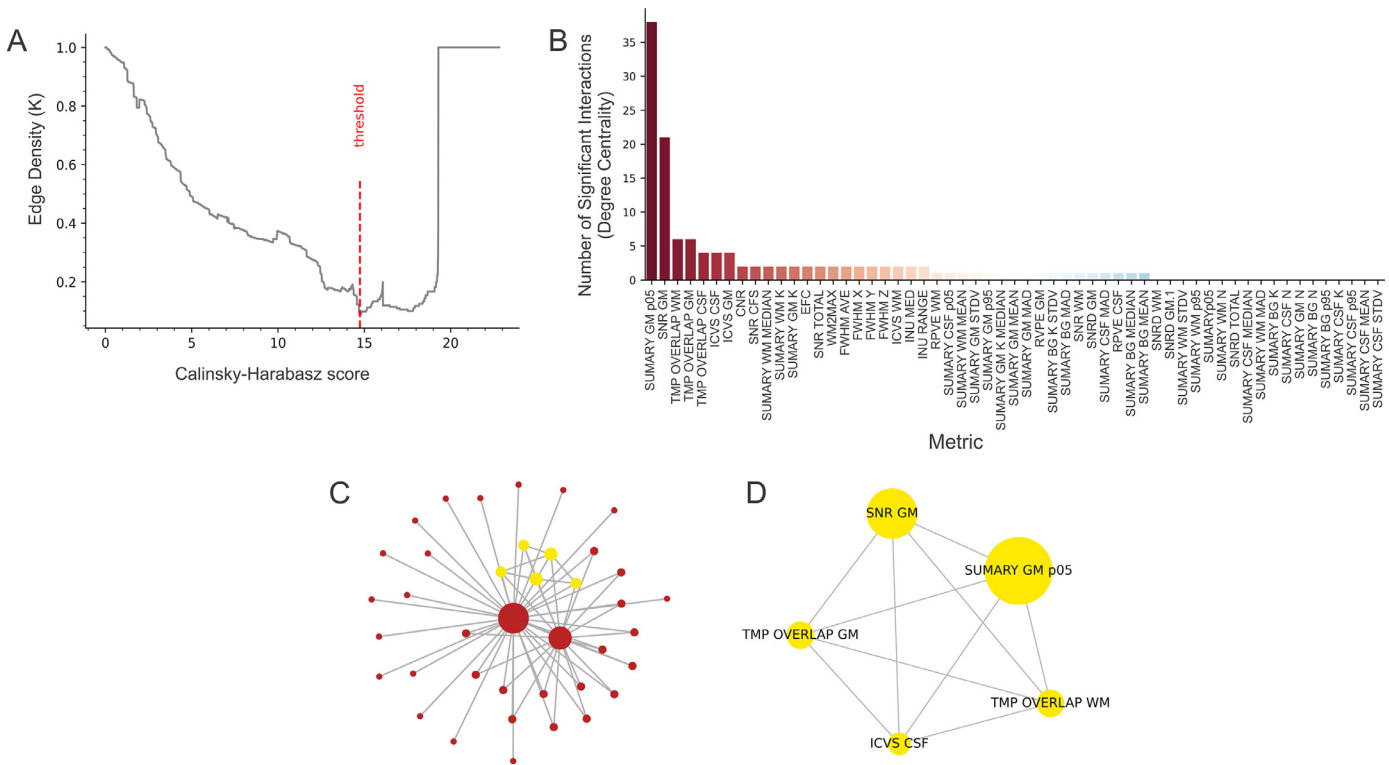

Fig. 3. Clustering evaluation. A. Calculation of the graph-extraction threshold using the edge density of graphs computed with the Calinski–Harabasz score. The red line corresponds to the threshold that minimized the edge density. B. Degree of centrality of all the IQMs as graph nodes. Note that only five IQMs show a large interrelation within the graph, indicating their large capability to dissociate the outcome-surfaces. C. Graph extracted at the threshold. D. Maximum clique.

Table 3

Metrics with significant node interactions that form a maximum clique with a high degree centrality.

Metric	Description	Value
Summary GM p05	Calculates the 5th percentile of the distribution of grey matter intensity.	Values closer to the median value indicate an accurate estimation of the gm (Esteban et al., 2017).
Signal to noise ratio (SNR GM)	Calculates the signal to noise ratio in the grey matter tissue.	Larger values are indicative of lower noise. Hence, higher values are preferred (Dietrich et al., 2007).
Tissue Probabilistic Mapping (TPM overlap WM and GM)	This metric calculates the overlap between the tissue probability maps estimated from the image and the probability maps calculated from the NMT template.	Values closer to 1 indicate a similarity to the template although deviating values may indicate inconsistencies in the image or individual image characteristics (Esteban et al., 2017).
Volume fraction (ICV CSF)	Estimation of the volume fraction of each tissue calculated on the FSL FAST's segmentation.	Normative values fall around 50%, 28% and 12% to GM/WM and CSF respectively (Seidlitz et al., 2018).
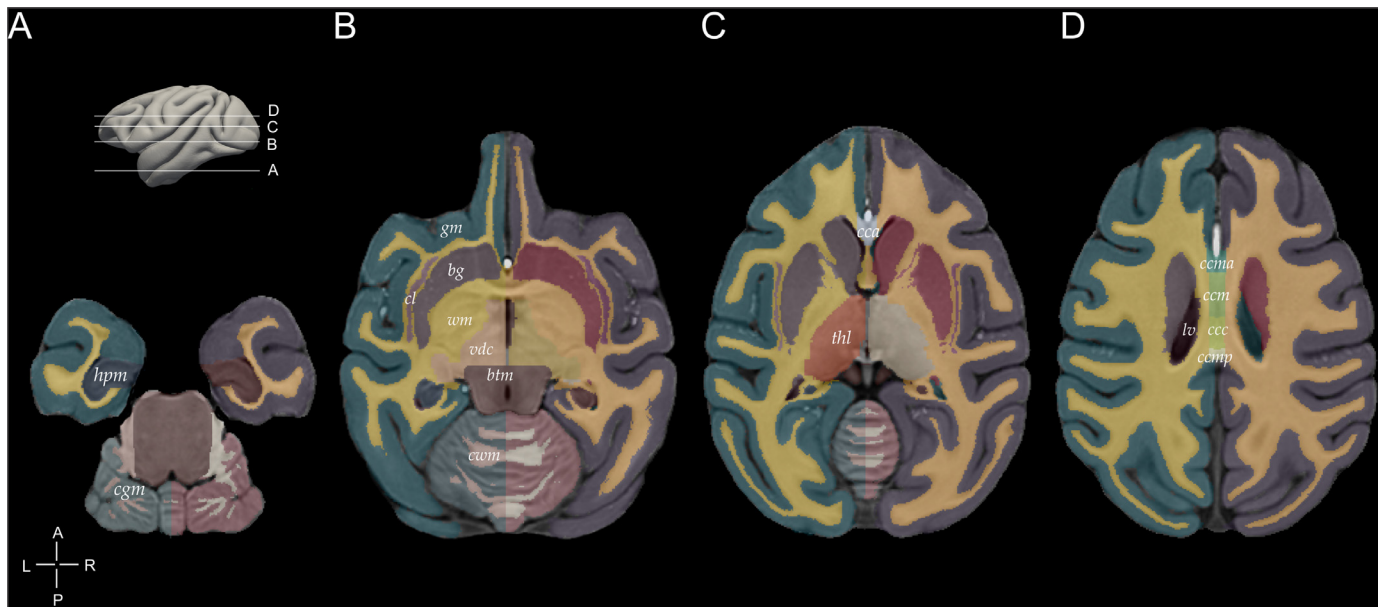
Fig. 4. PREEMACS FreeSurfer segmentation atlas. A–D. Axial sections of the brain at four dorsoventral levels shown in the inset of A. bg, basal ganglia; btm, brainstem; cca, anterior corpus callosum; ccma, mid anterior corpus callosum; ccm, mid corpus callosum; ccc, central corpus callosum; ccmp, mid posterior corpus callosum; cgm, cerebellar grey matter; cl, claustrum; cwm, cerebellar white matter; gm, grey matter; lv, lateral ventricle; hmp, hippocampus; thl, thalamus; vdc, ventral diencephalon; wm, white matter.

These IQMs were: Summary GM Percentile 5 (SgmP05), Signal to Noise Ratio of GM (SNR gm), Tissue Probabilistic Mapping to WM and GM (TMP wm/gm) and Volume Fraction of CSF (see Table 3, sorted by relevance). The SVMs using only these five IQMs showed an increase in performance to 72.8 ± 1.6%, supporting our hypothesis that critical IQMs can predict the PREEMAC outcome. This result also suggests that the remaining IQMs are features that do not contain information to predict the quality of the obtained surfaces and may even add noise to the classification procedure (Pavlidis et al., 2004).

3.4. PREEMACS FreeSurfer segmentation atlas

A custom monkey segmentation with macaque labels of cortical and subcortical structures was constructed to obtain an accurate surface estimation in Module 3. Fig. 4 shows the volumetric label estimation in NMT space. We estimated the volumes of subcortical structures from 57 monkey images using this segmentation atlas, available for downloading in a GitHub repository (https://github.com/pGarciaS/PREEMACS).

3.5. Registering the curvature and convexity: PREEMACS Rhesus parameterization file

To obtain the vertex correspondence between subjects and to compare anatomical features between animals, it is critical to align each monkey surface to a generic Rhesus reference template. We ran an iterative procedure on 33 monkey images (20 with minimum and 13 with medium surface errors, see below) to obtain a Rhesus monkey standard for the white matter curvature and convexity patterns, called PREEMACS Rhesus parameterization file (see Materials and Methods). This file includes nine parameters that fully characterize the geometry of the monkey cortical sulci. Fig. 5A shows the resulting mean curvature data pattern template warped in 2-D, which is one of the nine elements of the Rhesus parameterization file. Qualitatively, every expected sulcus is associated with a concave region in the warped pattern template (Fig. 5). All the subject surfaces were registered to this common space and can be expressed in a standard spherical coordinate system (i.e. longitude and latitude) to index a point on the folded cortical surface for a given subject. Supplementary Figs. 1 and 2 show the average isotopic (size-change) and average anisotropic (shape-change) distortions (Robinson et al., 2018) of twelve subjects (minimum errors in surface estimation from 6 PRIME-DE sites) when registered from native to a common space. Fig. 5 B–D shows lateral, mid-sagittal, and posterior views of the WM template surface as a unit sphere, defining the geometrical relation between all the sulci of a standard monkey brain. The template sphere is used to register all subjects for final surface analysis.

3.6. Average surfaces

The average wm and pial surfaces with 163,842 vertices per hemisphere are depicted in Figs. 6 and 7, respectively. The lateral, mid-
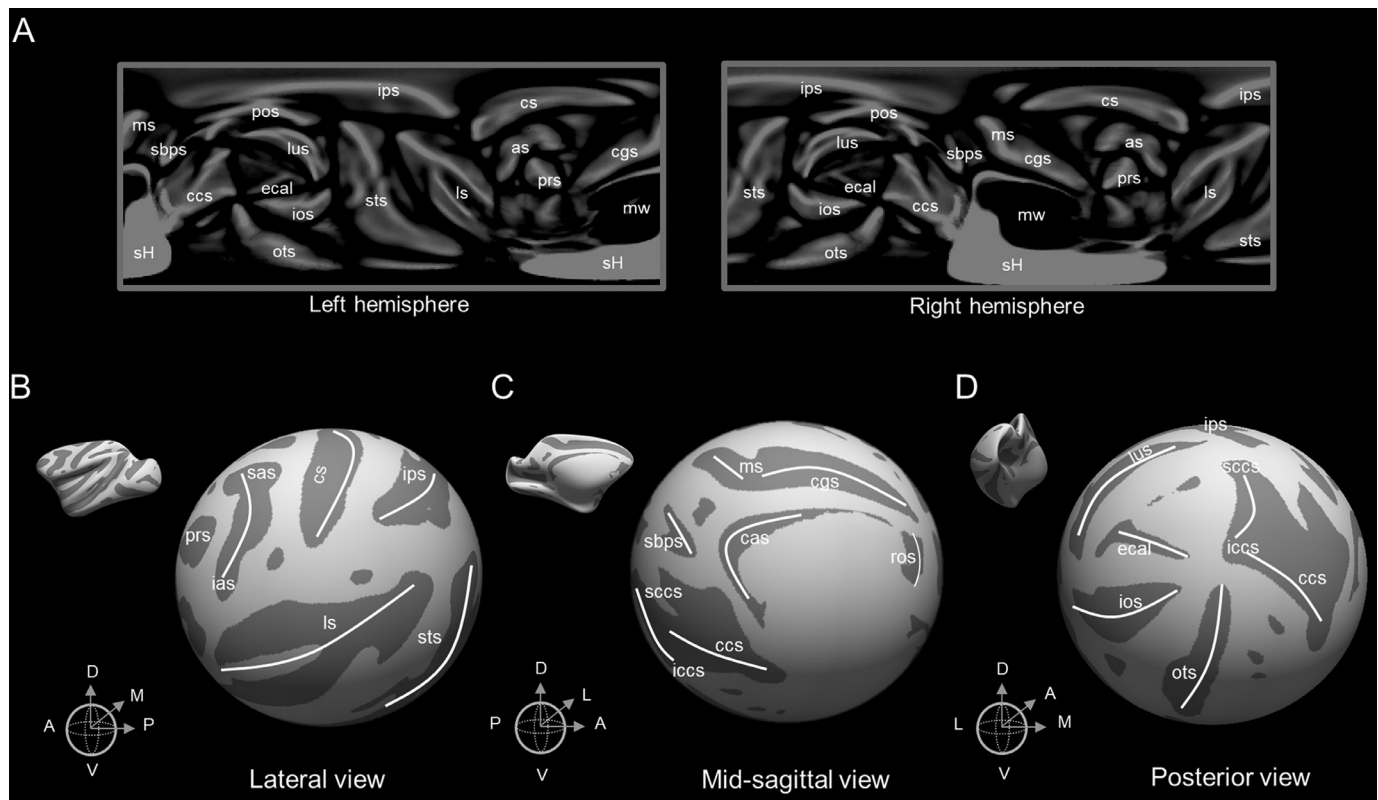
P. Garcia-Saldivar, A. Garimella, E.A. Garza-Villarreal et al.

NeuroImage 227 (2021) 117671

Fig. 5. PREEMACS Rhesus sphere and curvature pattern template. A. Mean curvature data pattern template warped in 2-D. This curvature data pattern is one of nine elements of the PREEMACS Rhesus parameterization file used as a template to align the surfaces and obtain vertex correspondence between the subjects. B, C and D. Left WM template surface inflated as a sphere (Lateral, Mid-sagittal, and Posterior view, respectively). Sulci labeled for reference: as, arcuate sulcus; cas, callosal sulcus; ccs, calcarine sulcus; cgs, cingulate sulcus; cs, central sulcus; ecal, external calcarine sulcus; ias, inferior arcuate sulcus; iccs, inferior calcarine sulcus; ios, inferior occipital sulcus; ips, intraparietal sulcus; ls, lateral sulcus; lus, lunate sulcus; ms, marginal sulcus; ots, occipitotemporal sulcus; pos, parietal-occipital sulcus; prs, principal sulcus; ros, rostral sulcus; sas, superior arcuate sulcus; sccs, superior calcarine sulcus; sbps, subparietal sulcus; sts, superior temporal sulcus; mw, medial wall; sH, space of hippocampus.

sagittal and ventral views of the surface templates show a high anatomical fidelity with an actual monkey brain, with no apparent artifacts in the curvature pattern across all sulci (Fig. 6) and gyri (Fig. 7). The individual wm and pial surfaces are registered to these templates for CT and gyrification analysis with a one-to-one vertex correspondence, which allows for further group analysis in a common Rhesus monkey space.

3.7. PREEMACS generalization and identification of surface errors

Fifty-seven sets of images from eleven different sites of the Primate Data Exchange (PRIME-DE) database were run with the PREEMACS pipeline. The resulting surfaces were evaluated for errors using a visual inspection test that included a criteria for smoothness of the surfaces and segmentation (see Section 2.2.2). Since the site accounts for a large source of variability between input images, we compared the test errors across the eleven sites (Fig. 8A). Notably, the surfaces of 20 (out of 57) monkey images from 8 sites showed minimal errors that needed negligible or no manual correction (Fig. 8A). The pial and wm surfaces of representative animals with minimal surface errors for five sites are shown in Fig. 8C. The most common segmentation errors (Fig. 8B) were located in the wm of Parahippocampal (Fig. 9A), Frontal Pole (Fig. 9B), Occipital Cortex (Fig. 9C) and Anterior cingulate cortex (Fig. 9D). The average time to correct these images by an expert using a manual correction toolbox from FreeSurfer was ~10 min. In addition, the surfaces of 13 and 30 subjects showed medium and large errors, respectively. Notably, these poor brain extractions were predicted from the IQMs classification analysis (Supplementary Fig. 3).

3.8. Cortical thickness

We computed the CT of the PREEMACS Rhesus average surface of the pial minus wm. It is evident in Fig. 10A that the monkey CT is not homogenous, with a thicker cortex in the frontal lobe, especially in the primary motor cortex, and a thinner cortex in the occipital lobe, corroborating previous results (Naselaris et al., 2006; Calabrese et al., 2015; Seidlitz et al., 2018). In addition, we compared the CT for the 662 vertices within the ROI in the left primary motor cortex (M1) depicted in Fig. 10B for the three outcome surface categories (minimum, medium or large errors) defined by the visual inspection test (see Section 2.2.2 "Quality control module"). The mean CT for this ROI was similar across outcome surface categories (five subjects per category, Fig. 10B). However, the dispersion of the CT was considerably larger for the surfaces with large segmentation errors (Fig. 10 B,C).

4. Discussion

4.1. PREEMACS strengths

PREEMACS is a robust, automatic, and flexible pipeline that standardizes all the needed steps, starting from raw structural MRI images, for the extraction of cortical surfaces in the macaque. The program has three modules: 1) preprocessing, 2) quality control and 3) brain surface estimation that are simple to run individually or as a complete image processing workflow.

Several key preprocessing steps have been fine-tuned in Module 1 to mitigate the severity of artifacts often seen in NHP imaging, such as
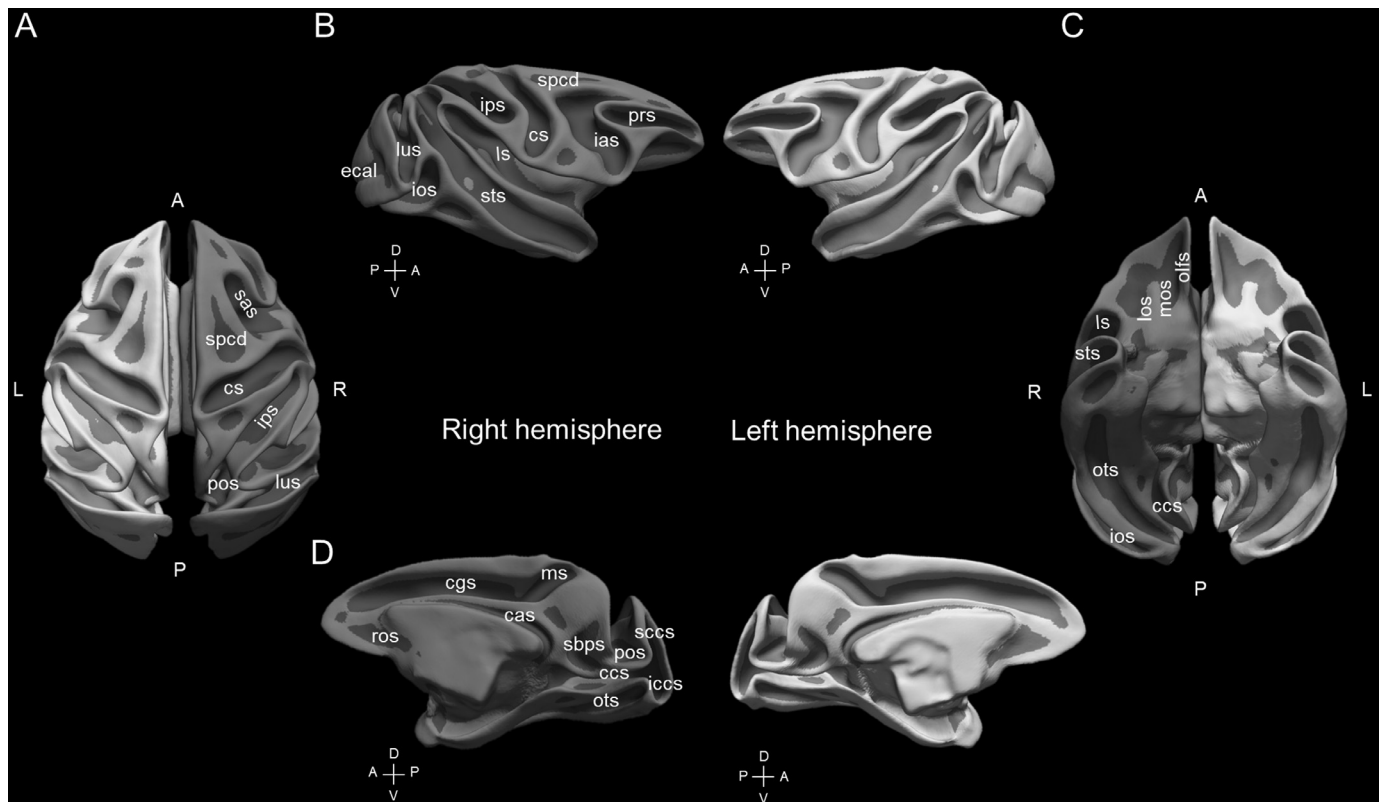
Fig. 6. PREEMACS Rhesus average WM surface showing the curvature data pattern. A. Dorsal view. B. Lateral view. C. Ventral view. D. Mid-sagittal view. Sulci labeled for reference: cas, callosal sulcus; ccs, calcarine sulcus; cgs, cingulate sulcus; cs, central sulcus; ecal, external calcarine sulcus; ias, inferior arcuate sulcus; iccs, inferior calcarine sulcus; ios, inferior occipital sulcus; ips, intraparietal sulcus; los, lateral orbital sulcus; ls, lateral sulcus; lus, lunate sulcus; ms, marginal sulcus; mos, medial orbital sulcus; olfs, olfatory sulcus; ots, occipitotemporal sulcus; pos, parietal-occipital sulcus; prs, principal sulcus; ros, rostral sulcus; sas, superior arcuate sulcus; sbps, subparietal sulcus; sccs, superior calcarine sulcus; spcd, superior precentral dimple; sts, superior temporal sulcus.

intensity non-uniformity (INU, due to coil sensitivity profiles and use of multi-channel array coils), skull stripping (with anatomy of NHP being vastly different from that of humans), and erroneous identification of dura as cortical tissue. Notably, our skull stripping method, based on a deep learning algorithm, obtains accurate brain masks with large DIC, sensitivity and specificity values, solving one of the most common bottlenecks in surface-based estimations.

The prior assessment of the image quality is fundamental for the automatic implementation of the present pipeline. Using different metrics from MRIqc, Module 2 provides an SVM classification method that predicts the quality of the resulting surfaces with a high degree of accuracy. This prediction tool was validated on 57 images of eleven sites. Crucially, the performed graph analysis indicates five IQMs are critical to predict PREEMACS surface outcome.

Three Rhesus monkey templates were developed for surface estimation in Module 3. The PREEMACS FreeSurfer segmentation atlas allows for the structural parcellation of cortical and subcortical structures improving the wm/gm segmentation. The PREEMACS Rhesus parameterization template includes all the information about the curvature and convexity patterns of the monkey wm. This template is crucial to obtain a vertex registration between subjects. Finally, the individual wm and pial surfaces are registered to the PREEMACS Rhesus average surface so that the CT and gyrification measures can be obtained for group analysis in a common Rhesus monkey space. Normalization is also needed to co-register individual brains onto multimodal atlases of interest, such as cytoarchitectonic, myeloarchitectonic, fiber tracking, etc., which can highly enrich the analytical potentiality of PREEMACS (Goubran et al., 2019). Therefore, these three templates provide a large specificity in the macaque surface estimation, with robust results across sites and image collection protocols.

Another strength of the present workflow is the accurate identification of the pial surface, which is achieved due to the combined information of T1w and T2w volumes. Nevertheless, is important to emphasize that PREEMACS offers the option to run the workflow on T1w only, although is highly recommended to use both input images for optimal results.

A fundamental characteristic of PREEMACS is that all images and the resulting surfaces are kept in native space, decreasing a large number of potential for biases due to local deformations at different image processing steps. Thus, PREEMACS can be also used for longitudinal data, obtaining surfaces automatically and easily producing subject-specific templates to preserve within-subject changes for final statistical analysis (Ashburner and Ridgway, 2013; Reuter et al., 2012).

4.2. PREEMACS generalizability

PREEMACS solves practically all the image preprocessing issues recently outlined by The PRIMatE-Data Exchange (PRIME-DE) Global Collaboration Workshop and Consortium (reference). Our pipeline generalized across a variety of input images performing properly the following steps: process images with different head orientations, performs an automatic cropping, can correct the strong intensity bias attributable to the huge variety of coils used, carries out an automatic skull stripping and performs an automatic tissue segmentation. Importantly, all these steps generalized across a dataset of images from eleven sites. Good surface reconstructions were obtained when the input images met the minimal IQMs criteria of our customized NHP quality control assessment. Specifically, images that had a voxel resolution of 0.5 mm^3, adequate SNR (specially for GM), and a large contrast between WM-GM showed proper segmentation and a good surface PREEMACS estimation. These
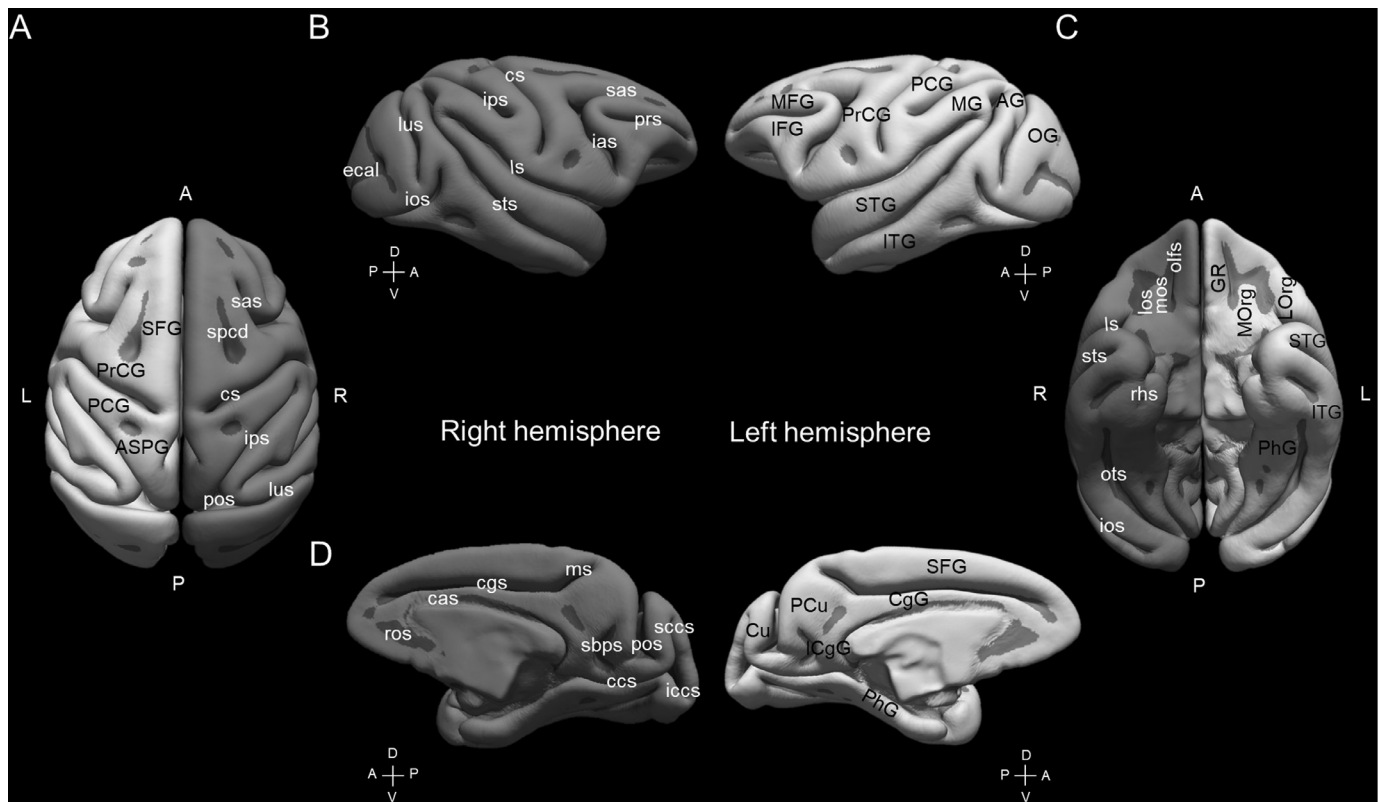
P. Garcia-Saldivar, A. Garimella, E.A. Garza-Villarreal et al.

NeuroImage 227 (2021) 117671

Fig. 7. PREEMACS Rhesus average pial surface showing the curvature data pattern. A. Dorsal view. B. Lateral view . C. Ventral view. D. Mid-sagittal view. Sulci and gyri are labeled for reference. Sulci: cas, callosal sulcus; ccs, calcarine sulcus; cgs, cingulate sulcus; cs, central sulcus; ecal, external calcarine sulcus; ias, inferior arcuate sulcus; iccs, inferior calcarine sulcus; ios, inferior occipital sulcus; ips, intraparietal sulcus; los, lateral orbital sulcus; ls, lateral sulcus; lus, lunate sulcus; ms, marginal sulcus; mos, medial orbital sulcus; olfs, olfactory sulcus; ots, occipitotemporal sulcus; pos, parietal-occipital sulcus; prs, principal sulcus; ros, rostral sulcus; rhs, rhinal sulcus; sas, superior arcuate sulcus; sbps, subparietal sulcus; sccs, superior calcarine sulcus; spcd, superior precentral dimple; sts, superior temporal sulcus. Gyri: SFG, superior frontal gyrus; AG, angular gyrus; ASPG, anterior superior parietal gyrus; CgG, cingulate gyrus; Cu, cuneus; GR, gyrus rectus; ICgG, isthmus of the cingulate gyrus; IFG, inferior frontal gyrus; ITG, inferior temporal gyrus; LOrg, lateral orbital gyrus; MG, marginal gyrus; MFG, middle frontal gyrus; MOrg, medial orbital gyrus; OG, occipital gyrus; PCG, postcentral gyrus; PCu, precuneus; PhG, parahippocampal gyrus; PrCG, precentral gyrus; STG, superior temporal gyrus.

exceptionally good results were obtained from 20 images independently of the MR scanner, the coil, and the monkey position (Supplementary Table 1). It is advisable that voxel resolution be high and isotropic, as surface estimation can only be as good as the lowest resolution available in the input volumes. In addition, the resulting CT was in the range of previously reported values (Georgopoulos et al., 2007; Calabrese et al., 2015; Seidlitz et al., 2018). Therefore, our validation provides an important piece of evidence for PREEMACS versatility and generalizability, ruling out any site effect in our tests.

4.3. Comparison with other pipelines for NHP surface reconstruction

As far as we know, five additional pipelines for NHP surface estimation exist (Messinger et al., 2021). These are HCP-style NHP Pipeline (Donahue et al., 2016; Donahue et al., 2018; Autio et al., 2020), CIVET-Macaque (Lepage et al., this issue), NHP-FreeSurfer, Precon_all, and Macapype, all of them contained in the Primate Resources Exchange (PRIME-RE) wiki (Messinger et al., 2021). All these tools for automatic extraction of cortical thickness in NHP show different levels of complexity, robustness, and automation. Due to scope constraints, we do not provide a formal quantitative comparison between pipelines. Qualitatively, the HCP-style NHP Pipeline has been validated across humans, chimpanzees, multiple monkey species, and marmosets (Glasser et al., 2013; Donahue et al., 2016; Donahue et al., 2018; Autio et al., 2020), and automatically identifies and labels the brain stem, cerebellum, and claustrum. Furthermore, this analytical environment includes additional

downstream features, such as structural, functional and diffusion image preprocessing tools. PREEMACS does not possess such features. The full description of CIVET-Macaque is part of this special issue on monkey MRI and shows similarities PREEMACS in its overall scope and utility. Both CIVET-Macaque and PREEMACS provide crucial adaptations and extensions of previously available processing pipelines for the estimation of cortical surfaces in humans, with the former relying on CIVET (Lepage et al., this issue) and the latter building on FreeSurfer. Notably, PREEMACS has a modular design, performs automatic and robust skull-striping through a convolutional neural network, carries out quality control assessment of input images, retains all image volumes and resulting surfaces in native space, uses custom made macaque templates within the pipeline, and (if input data is deemed of sufficient quality by the first module), is able to run fully automatically and provide cortical thickness data suitable for vertex-wise group analyses. In the spirit of collaboration and open science characteristic of PRIME-DE (Milham et al., 2020), we envision a close partnership between all groups working on NHP surface estimation (Messinger et al., 2021) to ultimately provide an integrated pipeline that dynamically evolves as the field grows.

4.4. Continuous updating of deep learning neuronal networks and SVMs

The PREEMACS brainmask tool was trained on 126 images from 18 PRIME-DE sites. The trained convolutional neural network model was quite robust, with predicted masks that showed close to perfect values for Dice, sensitivity and specificity. Nevertheless, an issue with
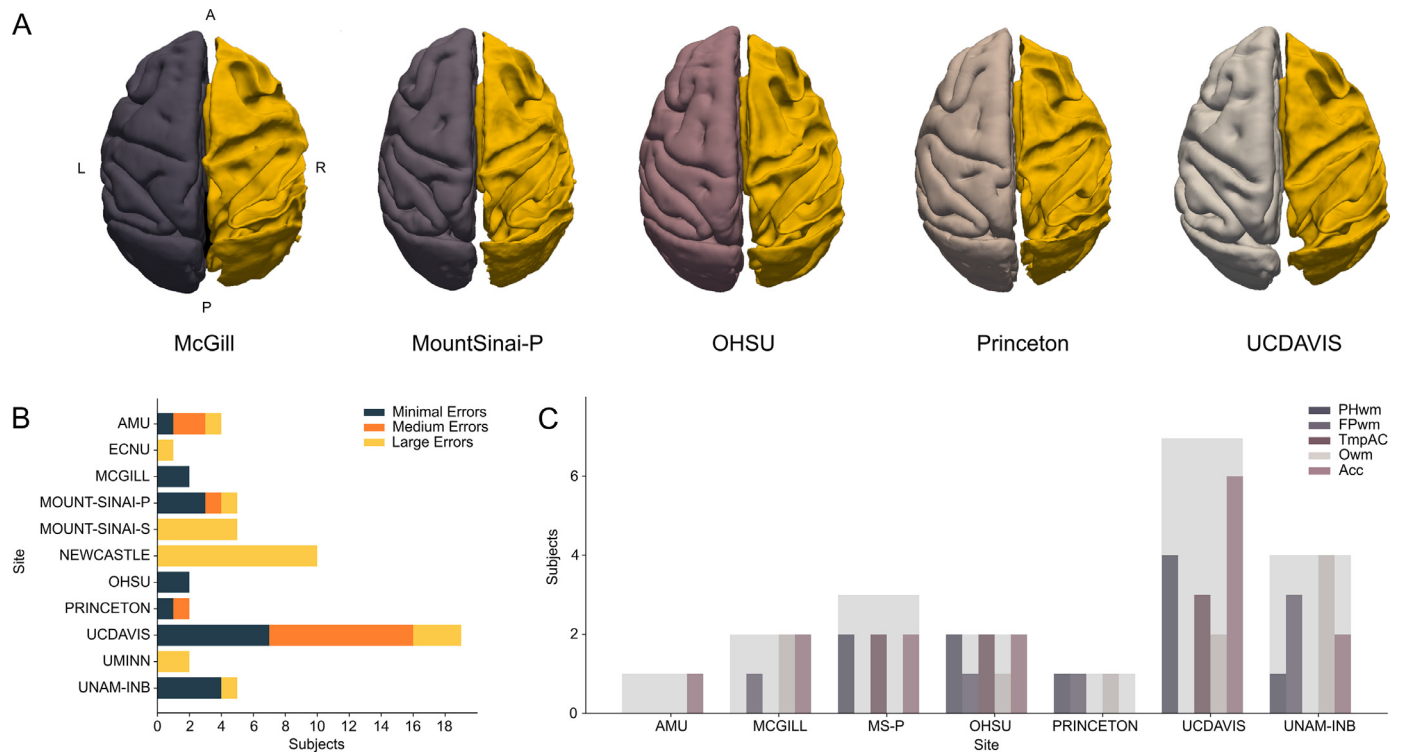
Fig. 8. Evaluation of errors in the PREEMACS cortical surfaces across sites. A. Pial (left) and wm (right) surfaces of representative monkeys with minimal surface errors for five sites labeled in the *x*-axis. B. Frequency of subjects with minimal, medium, and large errors in the PREEMACS cortical surfaces as a function of site ($n = 11$). C. Number of subjects with minimal errors in B that showed segmentation errors in five cortical areas across seven sites. The shaded grey area corresponds to the total number of subjects with minimal errors for each site; each subject can have one or more areas with minimal errors. PHwm, Parahippocampal wm; FPwm, Frontal Pole wm; TmpAC, Temporal anterior cortex; Owm, Occipital wm; Acc, Anterior cingulate cortex.
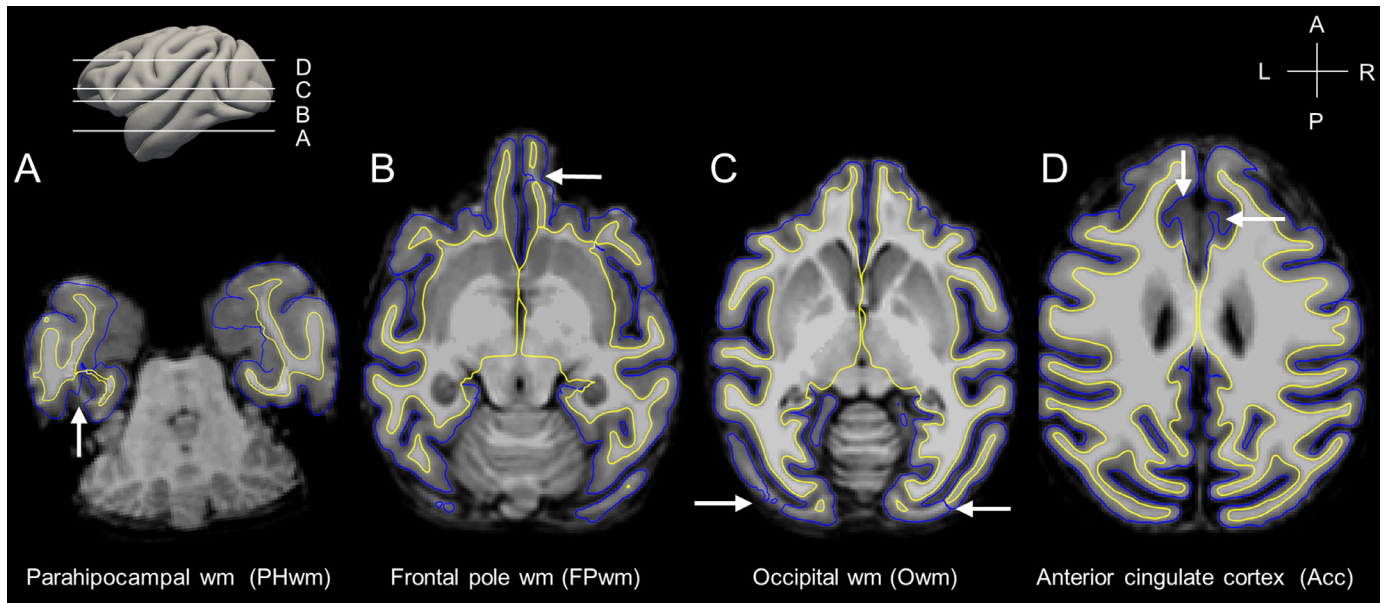
Fig. 9. Most common "minimal" segmentation errors. A. Parahippocampal wm (PHwm). B. Frontal Pole wm (FPwm) C. Occipital wm (Owm). D. Anterior cingulate cortex (Acc). Blue line for pial and yellow line for wm surface. Different individual shown in each panel.

model building is the generalizability of prediction for images collected with conditions not included in the original multidimensional space (Esteban et al., 2017). A similar problem is confronted on the SVM classification of fifty-seven surfaces based on the image metrics of our quality control routine. It is probable that no convergence has been obtained yet in these models due to the limited amount of input images and their constrained range of parameter values. Hence, these PREEMACS modules should be continuously updated and the models rebuilt until our skull-stripping and the quality control methods show robust performance for practically any image collection circumstance.
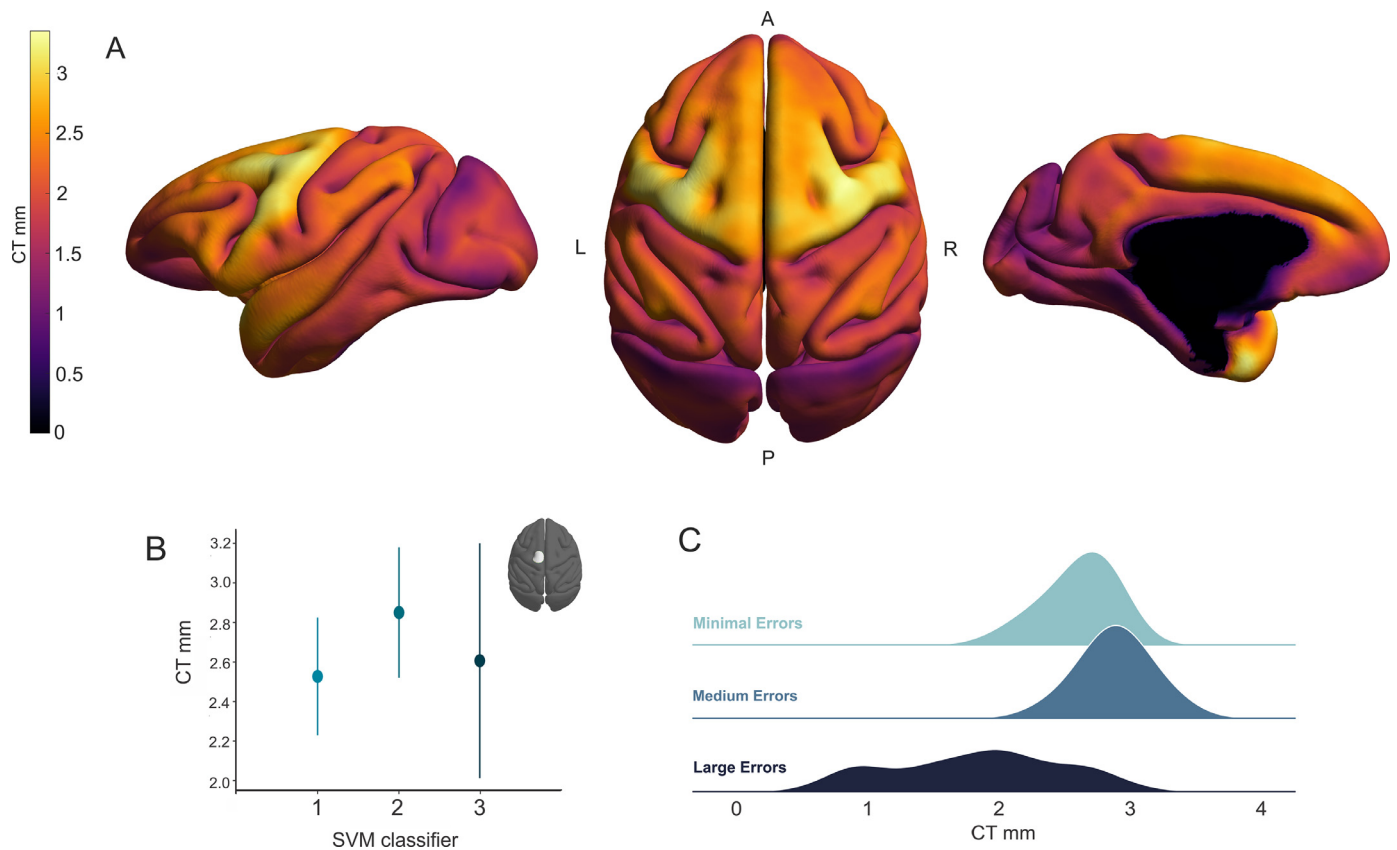
Fig. 10. Cortical thickness. A. Lateral, dorsal and medial views of the CT computed from the PREEMACS Rhesus average surfaces of pial minus wm shown in Figs. 6 and 7. B. Mean and standard deviation of the CT from five subjects pertaining to each of the three outcome surface categories (1 = minimum, 2 = medium or 3 = large errors) classified using the Visual Inspection Test. The inset shows the location of the ROI of the primary motor cortex used to compute the CT. C. Distribution of CT across all vertices in the M1 ROI for a representative subject from each of the three outcome surface categories.

4.5. PREEMACS limitations

Besides the potential lack of model convergence discussed above, PREEMACS does not include a macaque GCA atlas to parcellate in the FreeSurfer environment the corpus callosum, cerebellum and pons. Instead we use the human GCA atlas that produced some segmentation errors in the cerebellum and parts of visual cortex. In addition, there is no parcellation tool to identify cortical areas and automatically define ROIs for analysis between groups of animals.

5. Conclusion

PREEMACS is a new, flexible, versatile and robust pipeline for extraction of the Rhesus monkey cortical brain surface. The entire code is freely available at GitHub (https://github.com/PREEMACS/PREEMACS). The extraction of cortical surfaces in the macaque was performed with minimal or no manual intervention when the quality of the input images reached a certain threshold, showing a large success in surface reconstruction across the tested sites around the world. Considering the recent efforts toward data sharing in the non-human primate field (Milham et al., 2018), PREEMACS is a validated and user friendly pipeline for the automatic extraction of cortical surfaces, which can be used by the growing macaque neuroimaging community not only for cortical thickness estimation, but also to perform multimodal imaging analysis in the same geometrical space.

Data available

PREEMACS workflow code, manual brain masks, wm and pial surfaces, cortical ribbon and wm segmentation are available on https://github.com/pGarciaS/PREEMACS.

Declaration of Competing Interest

The authors declare no conflict of interest.

Credit authorship contribution statement

Pamela Garcia-Saldivar: Conceptualization, Methodology, Software, Validation, Formal analysis, Data curation, Visualization, Writing - original draft, Writing - review & editing. **Arun Garimella:** Methodology, Software, Formal analysis, Visualization, Writing - original draft, Writing - review & editing. **Eduardo A. Garza-Villarreal:** Methodology, Writing - original draft, Writing - review & editing. **Felipe A. Mendez:** Methodology, Software, Formal analysis, Writing - original draft, Writing - review & editing. **Hugo Merchant:** Conceptualization, Methodology, Formal analysis, Supervision, Project administration, Funding acquisition, Writing - original draft, Writing - review & editing.

P. Garcia-Saldivar, A. Garimella, E.A. Garza-Villarreal et al.

NeuroImage 227 (2021) 117671

Supplementary materials

Supplementary material associated with this article can be found, in the online version, at doi:10.1016/j.neuroimage.2020.117671.

References

Alfaro-Almagro, F., Jenkinson, M., Bangerter, N.K., Andersson, J.L.R., Griffanti, L., Douaud, G., Sotiropoulos, S.N., Jbabdi, S., Hernandez-Fernandez, M., Vallee, E., Vidaurre, D., Webster, M., McCarthy, P., Rorden, C., Daducci, A., Alexander, D.C., Zhang, H., Dragonu, I., Matthews, P.M., Miller, K.L., Smith, S.M., 2018. Image processing and quality control for the first 10,000 brain imaging datasets from UK Biobank. NeuroImage 166, 400–424. doi:10.1016/j.neuroimage.2017.10.034.

Ashburner, J., Ridgway, G.R., 2013. Symmetric diffeomorphic modeling of longitudinal structural MRI. Front. Neurosci. 6, 1–19. doi:10.3389/fnins.2012.00197.

Autio, J.A., Glasser, M.F., Ose, T., Donahue, C.J., Bastiani, M., Ohno, M., Kawabata, Y., Urushibata, Y., Murata, K., Nishigori, K., Yamaguchi, M., Hori, Y., Yoshida, A., Go, Y., Coalson, T.S., Jbabdi, S., Sotiropoulos, S.N., Kennedy, H., Smith, S., Essen, D.C.V., Hayashi, T., 2020. Towards HCP-style macaque connectomes: 24-channel 3T multi-array coil, MRI sequences and preprocessing. NeuroImage 215, 116800. http://doi.org/10.1016/j.neuroimage.2020.116800.

Avants, B.B., Tustison, N.J., Song, G., Cook, P.A., Klein, A., Gee, J.C., 2011. A reproducible evaluation of ANTs similarity metric performance in brain image registration. NeuroImage 54, 2033–2044. doi:10.1016/j.neuroimage.2010.09.025.

Avants, B., Dhillon, P., Kandel, B.M., Cook, P.A., McMillan, C.T., Grossman, M., Gee, J.C., 2012. Eigenanatomy improves detection power for longitudinal cortical change. In: Proceedings of the International Conference on Medical Image Computing and Computer-Assisted Intervention, Berlin, Heidelberg. Springer, pp. 206–213. doi:10.1007/978-3-642-33454-2_26.

Balbastre, Y., Rivière, D., Souedet, N., Fischer, C., Hérard, A.-S., Williams, S., Vandenberghe, M.E., Flament, J., Aron-Badin, R., Hantraye, P., Mangin, J.-F., Delzescaux, T., 2017. Primatologist: a modular segmentation pipeline for macaque brain morphometry. NeuroImage 162, 306–321. doi:10.1016/j.neuroimage.2017.09.007.

Beare, R., Chen, J., Adamson, C.L., Silk, T., Thompson, D.K., Yang, J.Y.M., A.anderson, V., Seal, M.L., G.wood, A., 2013. Brain extraction using the watershed transform from markers. Front. Neuroinform. 7, 1–15. doi:10.3389/fninf.2013.00032.

Buffalo, E.A., Movshon, J.A., Wurtz, R.H., 2019. From basic brain research to treating human brain disorders. Proc. Natl. Acad. Sci. 116, 26167–26172. doi:10.1073/pnas.1919895116.

Caminiti, R., Ghaziri, H., Galuske, R., Hof, P.R., Innocenti, G.M., 2009. Evolution amplified processing with temporally dispersed slow neuronal connectivity in primates. Proc. Natl. Acad. Sci. 106, 19551–19556. doi:10.1073/pnas.0907655106.

Calabrese, E., Badea, A., Coe, C.L., Lubach, G.R., Shi, Y., Styner, M.A., Johnson, G.A., 2015. A diffusion tensor MRI atlas of the postmortem rhesus macaque brain. NeuroImage 117, 408–416. doi:10.1016/j.neuroimage.2015.05.072.

Caliński, T., Harabasz, J., 1974. A dendrite method for cluster analysis. Commun. Stat.-Theory Methods 3 (1), 1–27. doi:10.1080/03610927408827101.

Cox, R.W., 1996. AFNI: software for analysis and visualization of functional magnetic resonance neuroimages. Comput. Biomed. Res. 29, 162–173. doi:10.1006/cbmr.1996.0014.

Crowe, D.A., Zarco, W., Bartolo, R., Merchant, H., 2014. Dynamic representation of the temporal and sequential structure of rhythmic movements in the primate medial premotor cortex. J. Neurosci. 34 (36), 11972–11983. doi:10.1523/JNEUROSCI.2177-14.2014.

Dale, A.M., Fischl, B., Sereno, M.I., 1999. Cortical surface-based analysis. I. Segmentation and surface reconstruction. NeuroImage 9, 179–194. doi:10.1006/nimg.1998.0395.

Davatzikos, C., Bhatt, P., Shaw, L.M., Batmanghelich, K.N., Trojanowski, J.Q., 2011. Prediction of MCI to AD conversion, via MRI, CSF biomarkers, and pattern classification. Neurobiol. Aging 32, 2322. doi:10.1016/j.neurobiolaging.2010.05.023.

Dice, L.R., 1945. Measures of the amount of ecologic association between species author. Ecology 26 (3), 297–302.

Dietrich, O., Raya, J.G., Reeder, S.B., Reiser, M.F., Schoenberg, S.O., 2007. Measurement of signal-to-noise ratios in MR images: influence of multichannel coils, parallel imaging, and reconstruction filters. J. Magn. Reson. Imaging 26 (2), 375–385. doi:10.1002/jmri.20969.

Donahue, C.J., Sotiropoulos, S.N., Jbabdi, S., Hernandez-Fernandez, M., Behrens, T.E., Dyrby, T.B., Coalson, T., Kennedy, H., Knoblauch, K., Van Essen, D.C., Glasser, M.F., 2016. Using diffusion tractography to predict cortical connection strength and distance: a quantitative comparison with tracers in the monkey. J. Neurosci. 36 (25), 6758–6770. doi:10.1523/JNEUROSCI.0493-16.2016.

Donahue, C.J., Glasser, M.F., Preuss, T.M., Rilling, J.K., Van Essen, D.C., 2018. Quantitative assessment of prefrontal cortex in humans relative to nonhuman primates. Proc. Natl. Acad. Sci. 115, 5183–5192. doi:10.1073/pnas.1721653115.

Ducharme, S., Albaugh, M.D., Nguyen, T.V., Hudziak, J.J., Mateos-Pérez, J.M., Labbe, A., Evans, A.C., Karama, S.Brain Development Cooperative Group, 2016. Trajectories of cortical thickness maturation in normal brain development – the importance of quality control procedures. NeuroImage 125, 267–279. doi:10.1016/j.neuroimage.2015.10.010.

Eggert, L.D., Sommer, J., Jansen, A., Kircher, T., Konrad, C., 2012. Accuracy and reliability of automated gray matter segmentation pathways on real and simulated structural magnetic resonance images of the human brain. PLoS One 7 (9). doi:10.1371/journal.pone.0045081.

Eskildsen, S.F., Coupé, P., Fonov, V., Manjón, J.V., Leung, K.K., Guizard, N., Wassef, S.N., Østergaard, L.R., Collins, D.L., 2012. BEaST: brain extraction based on nonlocal segmentation technique. NeuroImage 59 (3), 2362–2373. doi:10.1016/j.neuroimage.2011.09.012.

Esteban, O., Birman, D., Schaer, M., Koyejo, O.O., Poldrack, R.A., Gorgolewski, K.J., 2017. MRIQC: advancing the automatic prediction of image quality in MRI from unseen sites. PLoS One 12, 1–21. doi:10.1371/journal.pone.0184661.

Esteban, O., Markiewicz, C.J., Blair, R.W., Moodie, C.A., Isik, A.I., Erramuzpe, A., Kent, J.D., Goncalves, M., DuPre, E., Snyder, M., Oya, H., Ghosh, S.S., Wright, J., Durnez, J., Poldrack, R.A., Gorgolewski, K.J., 2019. fMRIPrep: a robust preprocessing pipeline for functional MRI. Nat. Methods 16, 111–116. doi:10.1038/s41592-018-0235-4.

Fischl, B., Martin, I.S., Roger, B.H.T., Anders, M.D., 1999a. High-resolution intersubject averaging and a coordinate system for the cortical surface. Hum. Brain Mapp. 8 272–284. https://doi.org/10.1002/(SICI)1097-0193(1999)8:4<272::AID-HBM10>3.0.CO;2-4.

Fischl, B., Sereno, M.I., Dale, A.M., 1999b. Cortical surface-based analysis. II: Inflation, flattening, and a surface-based coordinate system. NeuroImage 9, 195–207. doi:10.1006/nimg.1998.0396.

Fischl, B., Salat, D.H., Busa, E., Albert, M., Dieterich, M., Haselgrove, C., van der Kouwe, A., Killiany, R., Kennedy, D., Klaveness, S., Montillo, A., Makris, N., Rosen, B., Dale, A.M., 2002. Whole brain segmentation. Neuron 33 (3), 341–355. doi:10.1016/s0896-6273(02)00569-x.

Fischl, B., 2012. FreeSurfer. NeuroImage 62, 774–781. doi:10.1016/j.neuroimage.2012.01.021.

Fortes, A.F., Merchant, H., Georgopoulos, A.P., 2004. Comparative and categorical spatial judgments in the monkey: "high" and "low. Anim. Cognit. 7 (2), 101–108. doi:10.1007/s10071-003-0195-6.

Galvan, A., Stauffer, W.R., Acker, L., El-Shamayleh, Y., Inoue, K., Ohayon, S., Schmid, M.C., 2017. Nonhuman primate optogenetics: recent advances and future directions. J. Neurosci. 37, 10894–10903. doi:10.1523/JNEUROSCI.1839-17.2017.

Georgopoulos, A.P., Merchant, H., Naselaris, T., Amirikian, B., 2007. Mapping of the preferred direction in the motor cortex. Proc. Natl. Acad. Sci. U.S.A. 104 (26), 11068–11072. doi:10.1073/pnas.0611597104.

Glasser, M.F., Sotiropoulos, S.N., Wilson, J.A., Coalson, T.S., Fischl, B., Andersson, J.L., Xu, J., Jbabdi, S., Webster, M., Polimeni, J.R., Van Essen, D.C., Jenkinson, M., 2013. The minimal preprocessing pipelines for the human connectome project. NeuroImage 80, 105–124. doi:10.1016/j.neuroimage.2013.04.127.

Goldberg, M.E., 2019. The neurology clinic needs monkey research. Proc. Natl. Acad. Sci. 116, 26255–26258. doi:10.1073/pnas.1907759116.

Goubran, M., Leuze, C., Hsueh, B., Aswendt, M., Ye, L., Tian, Q., Cheng, M.Y., Crow, A., Steinberg, G.K., McNab, J.A., Deisseroth, K., Zeineh, M., 2019. Multimodal image registration and connectivity analysis for integration of connectomic data from microscopy to MRI. Nat. Commun. 10 (1), 1–17. doi:10.1038/s41467-019-13374-0.

Gronenschild, E.H.B.M., Habets, P., Jacobs, H.I.L., Mengelers, R., Rozendaal, N., van Os, J., Marcelis, M., 2012. The effects of FreeSurfer version, workstation type, and Macintosh operating system version on anatomical volume and cortical thickness measurements. PLoS One 7 (6). doi:10.1371/journal.pone.0038234.

Iglesias, J.E., Liu, C.Y., Thompson, P.M., Tu, Z., 2011. Robust brain extraction across datasets and comparison with publicly available methods. IEEE Trans. Med. Imaging 30 (9), 1617–1634. doi:10.1109/TMI.2011.2138152.

Itzcovich, I., 2017. DeepBrain. Instituto Tecnológico de Buenos Aires, Buenos Aires, Argentina. https://github.com/iitzco. Available at: https://github.com/iitzco/deepbrain.

Klapwijk, E.T., van de Kamp, F., van der Meulen, M., Peters, S., Wierenga, L.M., 2019. Qoala-T: a supervised-learning tool for quality control of FreeSurfer segmented MRI data. NeuroImage 189, 116–129. doi:10.1016/j.neuroimage.2019.01.014.

Kim, J.S., Singh, V., Lee, J.K., Lerch, J., Ad-Dab'bagh, Y., MacDonald, D., Lee, J.M., Kim, S.I., Evans, A.C., 2005. Automated 3-D extraction and evaluation of the inner and outer cortical surfaces using a Laplacian map and partial volume effect classification. NeuroImage 27, 210–221. doi:10.1016/j.neuroimage.2005.03.036.

Kleesiek, J., Urban, G., Hubert, A., Schwarz, D., Maier-Hein, K., Bendszus, M., Biller, A., 2016. Deep MRI brain extraction: a 3D convolutional neural network for skull stripping. NeuroImage 129, 460–469. doi:10.1016/j.neuroimage.2016.01.024.

Lerch, J.P., van der Kouwe, A.J.W., Raznahan, A., Paus, T., Johansen-Berg, H., Miller, K.L., Smith, S.M., Fischl, B., Sotiropoulos, S.N., 2017. Studying neuroanatomy using MRI. Nat. Neurosci. 20, 314–326. doi:10.1038/nn.4501.

Li, G., Liu, T., Ni, D., Lin, W., Gilmore, J.H., Shen, D., 2015. Spatiotemporal patterns of cortical fiber density in developing infants, and their relationship with cortical thickness. Hum. Brain Mapp. 36, 5183–5195. doi:10.1002/hbm.23003.

Li, M., Liu, F., Jiang, H., Lee, T.S., Tang, S., 2017. Long-term two-photon imaging in awake macaque monkey. Neuron 93, 1049–1057. doi:10.1016/j.neuron.2017.01.027.

Lohmeier, J., Kaneko, T., Hamm, B., Makowski, M.R., Okano, H., 2019. atlasBREX: automated template-derived brain extraction in animal MRI. Sci. Rep. 9, 1–9. doi:10.1038/s41598-019-48489-3.

Manjón, J.V., Eskildsen, S.F., Coupé, P., Romero, J.E., Collins, D.L., Robles, M., 2014. Nonlocal intracranial cavity extraction. Int. J. Biomed. Imaging 2014, 1–11. doi:10.1155/2014/820205.

Mendoza, G., Merchant, H., 2014. Motor system evolution and the emergence of high cognitive functions. Prog. Neurobiol. 122, 73–93. doi:10.1016/j.pneurobio.2014.09.001.

Mendoza, G., Peyrache, A., Gámez, J., Prado, L., Buzsáki, G., Merchant, H., 2016. Recording extracellular neural activity in the behaving monkey using a

semichronic and high-density electrode system. J. Neurophysiol. 116, 563–574. doi:10.1152/jn.00116.2016.

Merchant, H., Grahn, J., Trainor, L., Rohrmeier, M., Fitch, W.T., 2015. Finding the beat: a neural perspective across humans and non-human primates. Philos. Trans. R. Soc. B: Biol. Sci. 370 (1664), 20140093. doi:10.1098/rstb.2014.0093, https://.

Merchant, H., Averbeck, B.B., 2017. The computational and neural basis of rhythmic timing in medial premotor cortex. J. Neurosci. 37 (17). doi:10.1523/JNEUROSCI.0367-17.2017.

Messinger, A., Sirmpilatze, N., Heuer, K., Kee, K., Mars, R.B., Sein, J., Xu, T., Glen, D., Jung, B., Seidlitz, J., Taylor, P., Toro, R., Garza-Villarreal, E.A., Sponheim, C., Wang, X., Benn, R.A., Cagna, B., Dadarwal, R., Evrard, H.C., García-Saldivar, P., Giavasis, S., Hartig, R., Lepage, C., Liu, C., Majka, P., Merchant, H., Milham, M.P., Rosa, M.G.P., Tasserie, J., Uhrig, L., Margulies, D.S., Klink, P.C., 2021. A collaborative resource platform for non-human primate neuroimaging. NeuroImage 226, 117519. doi:10.1016/j.neuroimage.2020.117519.

Milham, M., Petkov, C.I., Margulies, D.S., Schroeder, C.E., Basso, M.A., Belin, P., Fair, D.A., Fox, A., Kastner, S., Mars, R.B., Messinger, A., Poirier, C., Vanduffel, W., Van Essen, D.C., Alvand, A., Becker, Y., Ben Hamed, S., Benn, A., Bodin, C., Boretius, S., Cagna, B., Coulon, O., El-Gohary, S.H., Evrard, H., Forkel, S.J., Friedrich, P., Froudist-Walsh, S., Garza-Villarreal, E.A., Gao, Y., Gozzi, A., Grigis, A., Hartig, R., Hayashi, T., Heuer, K., Howells, H., Ardesch, D.J., Jarraya, B., Jarrett, W., Jedema, H.P., Kagan, I., Kelly, C., Kennedy, H., Klink, P.C., Kwok, S.C., Leech, R., Liu, X., Madan, C., Madushanka, W., Majka, P., Mallon, A.-M., Marche, K., Meguerditchian, A., Menon, R.S., Merchant, H., Mitchell, A., Nenning, K.-H., Nikolaidis, A., Ortiz-Rios, M., Pagani, M., Pareek, V., Prescott, M., Procyk, E., Rajimehr, R., Rautu, I.-S., Raz, A., Roe, A.W., Rossi-Pool, R., Roumazeilles, L., Sakai, T., Sallet, J., García-Saldivar, P., Sato, C., Sawiak, S., Schiffer, M., Schwiedrzik, C.M., Seidlitz, J., Sein, J., Shen, Z., Shmuel, A., Silva, A.C., Simone, L., Sirmpilatze, N., Sliwa, J., Smallwood, J., Tasserie, J., Thiebaut de Schotten, M., Toro, R., Trapeau, R., Uhrig, L., Vezoli, J., Wang, Z., Wells, S., Williams, B., Xu, T., Xu, A.G., Yacoub, E., Zhan, M., Ai, L., Amiez, C., Balezeau, F., Baxter, M.G., Blezer, E.L.A., Brochier, T., Chen, A., Croxson, P.L., Damatac, C.G., Dehaene, S., Everling, S., Fleysher, L., Freiwald, W., Griffiths, T.D., Guedj, C., Hadj-Bouziane, F., Harel, N., Hiba, B., Jung, B., Koo, B., Laland, K.N., Leopold, D.A., Lindenfors, P., Meunier, M., Mok, K., Morrison, J.H., Nacef, J., Nagy, J., Pinsk, M., Reader, S.M., Roelfsema, P.R., Rudko, D.A., Rushworth, M.F.S., Russ, B.E., Schmid, M.C., Sullivan, E.L., Thiele, A., Todorov, O.S., Tsao, D., Ungerleider, L., Wilson, C.R.E., Ye, F.Q., Zarco, W., Zhou, Y., 2020. Accelerating the evolution of nonhuman primate neuroimaging. Neuron 105, 600–603. doi:10.1016/j.neuron.2019.12.023.

Milham, M.P., Ai, L., Koo, B., Xu, T., Amiez, C., Balezeau, F., Baxter, M.G., Blezer, E.L.A., Brochier, T., Chen, A., Croxson, P.L., Damatac, C.G., Dehaene, S., Everling, S., Fair, D.A., Fleysher, L., Freiwald, W., Froudist-Walsh, S., Griffiths, T.D., Guedj, C., Hadj-Bouziane, F., Ben Hamed, S., Harel, N., Hiba, B., Jarraya, B., Jung, B., Kastner, S., Klink, P.C., Kwok, S.C., Laland, K.N., Leopold, D.A., Lindenfors, P., Mars, R.B., Menon, R.S., Messinger, A., Meunier, M., Mok, K., Morrison, J.H., Nacef, J., Nagy, J., Rios, M.O., Petkov, C.I., Pinsk, M., Poirier, C., Procyk, E., Rajimehr, R., Reader, S.M., Roelfsema, P.R., Rudko, D.A., Rushworth, M.F.S., Russ, B.E., Sallet, J., Schmid, M.C., Schwiedrzik, C.M., Seidlitz, J., Sein, J., Shmuel, A., Sullivan, E.L., Ungerleider, L., Thiele, A., Todorov, O.S., Tsao, D., Wang, Z., Wilson, C.R.E., Yacoub, E., Ye, F.Q., Zarco, W., Zhou, Y., Margulies, D.S., Schroeder, C.E., 2018. An open resource for non-human primate imaging. Neuron 100, 61–74. doi:10.1016/j.neuron.2018.08.039, e2https://doi.org/.

Miller, M.I., Massie, A.B., Ratnanather, J.T., Botteron, K.N., Csernansky, J.G., 2000. Bayesian construction of geometrically based cortical thickness metrics. NeuroImage 12, 676–687. doi:10.1006/nimg.2000.0666.

Bedford, S.A., Park, M.T.M., Devenyi, G.A., Tullo, S., Germann, J., Patel, R., Anagnostou, E., Baron-Cohen, S., Bullmore, E.T., Chura, L.R., Craig, M.C., Ecker, C., Floris, D.L., Holt, R.J., Lenroot, R., Lerch, J.P., Lombardo, M.V., Murphy, D.G.M., Raznahan, A., Ruigrok, A.N.V., Smith, E., Spencer, M.D., Suckling, J., Taylor, M.J., Thurm, A., Lai, M.-C., Chakravarty, M.M.MRC AIMS Consortium, 2019. Large-scale analyses of the relationship between sex, age and intelligence quotient heterogeneity and cortical morphometry in autism spectrum disorder. Mol. Psychiatry doi:10.1038/s41380-019-0420-6.

Naselaris, T., Merchant, H., Amirikian, B., Georgopoulos, A.P., 2005. Spatial reconstruction of trajectories of an array of recording microelectrodes. J. Neurophysiol. 93, 2318–2330. doi:10.1152/jn.00581.2004.

Naselaris, T., Merchant, H., Amirikian, B., Georgopoulos, A.P., 2006. Large-scale organization of preferred directions in the motor cortex. II. Analysis of local distributions. J. Neurophysiol. 96 (6), 3237–3247. doi:10.1152/jn.00488.2006.

Oguz, I., Styner, M., Sanchez, M., Shi, Y., Sonka, M., 2015. LOGISMOS-B for primates: primate cortical surface reconstruction and thickness measurement. Medical Imaging 2015: Image Processing, 9413. International Society for Optics and Photonics doi:10.1117/12.2082327.

Pavlidis, P., Wapinski, I., Noble, W.S., 2004. Support vector machine classification on the web. Bioinformatics 20 (4), 586–587. doi:10.1093/bioinformatics/btg461.

Reuter, M., Schmansky, N.J., Rosas, H.D., Fischl, B., 2012. Within-subject template estimation for unbiased longitudinal image analysis. NeuroImage 61 (4), 1402–1418. doi:10.1016/j.neuroimage.2012.02.084.

Rilling, J., Glasser, M., Jbabdi, S., Andersson, J., Preuss, T., 2012. Continuity, divergence, and the evolution of brain language pathways. Front. Evolut. Neurosci. 3, 1–6. doi:10.3389/fnevo.2011.00011.

Robinson, E.C., Garcia, K., Glasser, M.F., Chen, Z., Coalson, T.S., Makropoulos, A., Bozek, J., Wright, R., Schuh, A., Webster, M., Hutter, J., Price, A., Cordero Grande, L., Hughes, E., Tusor, N., Bayly, P.V., Van Essen, D.C., Smith, S.M., Edwards, A.D., Hajnal, J., Jenkinson, M., Glocker, B., Rueckert, D., 2018. Multimodal surface

matching with higher-order smoothness constraints. NeuroImage 167, 453–465. doi:10.1016/j.neuroimage.2017.10.037.

Rosen, A.F.G., Roalf, D.R., Ruparel, K., Blake, J., Seelaus, K., Villa, L.P., Ciric, R., Cook, P.A., Davatzikos, C., Elliott, M.A., Garcia de La Garza, A., Gennatas, E.D., Quarmley, M., Schmitt, J.E., Shinohara, R.T., Tisdall, M.D., Craddock, R.C., Gur, R.E., Gur, R.C., Satterthwaite, T.D, 2018. Quantitative assessment of structural image quality. NeuroImage 169, 407–418. doi:10.1016/j.neuroimage.2017.12.059.

Royer, L., Reimann, M., Andreopoulos, B., Schroeder, M., 2008. Unraveling protein networks with power graph analysis. PLoS Comput. Biol. 4 (7). doi:10.1371/journal.pcbi.1000108.

Rueda, A., Acosta, O., Couprie, M., Bourgeat, P., Fripp, J., Dowson, N., Romero, E., Salvado, O., 2010. Topology-corrected segmentation and local intensity estimates for improved partial volume classification of brain cortex in MRI. J. Neurosci. Methods 188, 305–315. doi:10.1016/j.jneumeth.2010.02.020.

Sampaio-Baptista, C., Johansen-Berg, H., 2017. White matter plasticity in the adult brain. Neuron 96 (6), 1239–1251. doi:10.1016/j.neuron.2017.11.026.

Scholtens, L.H., de Reus, M.A., van den Heuvel, M.P., 2015. Linking contemporary high resolution magnetic resonance imaging to the von economo legacy: a study on the comparison of MRI cortical thickness and histological measurements of cortical structure. Hum. Brain Mapp. 36, 3038–3046. doi:10.1002/hbm.22826.

Schwarz, D.A., Lebedev, M.A., Hanson, T.L., Dimitrov, D.F., Lehew, G., Meloy, J., Rajangam, S., Subramanian, V., Ifft, P.J., Li, Z., Ramakrishnan, A., Tate, A., Zhuang, K.Z., Nicolelis, M.A.L, 2014. Chronic, wireless recordings of large-scale brain activity in freely moving rhesus monkeys. Nat. Methods 11 (6), 670–676. doi:10.1038/nmeth.2936.

Scott, J.A., Grayson, D., Fletcher, E., Lee, A., Bauman, M.D., Schumann, C.M., Buonocore, M.H., Amaral, D.G., 2016. Longitudinal analysis of the developing rhesus monkey brain using magnetic resonance imaging: birth to adulthood. Brain Struct. Funct. 221, 2847–2871. doi:10.1007/s00429-015-1076-x.

Seidlitz, J., Sponheim, C., Glen, D., Ye, F.Q., Saleem, K.S., Leopold, D.A., Ungerleider, L., Messinger, A., 2018. A population MRI brain template and analysis tools for the macaque. NeuroImage 170, 121–131. doi:10.1016/j.neuroimage.2017.04.063.

Shaw, P., Kabani, N.J., Lerch, J.P., Eckstrand, K., Lenroot, R., Gogtay, N., Greenstein, D., Clasen, L., Evans, A., Rapoport, J.L., Giedd, J.N., Wise, S.P., 2008. Neurodevelopmental trajectories of the human cerebral cortex. J. Neurosci. 28, 3586–3594. doi:10.1523/JNEUROSCI.5309-07.2008.

Smith, S.M., 2002. Fast robust automated brain extraction. Hum. Brain Mapp. 17 (3), 143–155. doi:10.1002/hbm.10062.

Smith, S.M., Jenkinson, M., Woolrich, M.W., Beckmann, C.F., Behrens, T.E.J., Johansen-Berg, H., Bannister, P.R., De Luca, M., Drobnjak, I., Flitney, D.E., Niazy, R.K., Saunders, J., Vickers, J., Zhang, Y., De Stefano, N., Brady, J.M., Matthews, P.M., 2004. Advances in functional and structural MR image analysis and implementation as FSL. NeuroImage 23, 208–219. doi:10.1016/j.neuroimage.2004.07.051.

Sultan, F., Hamodeh, S., Murayama, Y., Saleem, K.S., Logothetis, N., 2010. Flat map areal topography in Macaca mulatta based on combined MRI and histology. Magn. Reson. Imaging 28, 1159–1164. doi:10.1016/j.mri.2010.03.023.

Tournier, J.-D., Smith, R., Raffelt, D., Tabbara, R., Dhollander, T., Pietsch, M., Christiaens, D., Jeurissen, B., Yeh, C.-H., Connelly, A., 2019. MRtrix3: a fast, flexible and open software framework for medical image processing and visualisation. NeuroImage 202, 116–137. doi:10.1016/j.neuroimage.2019.116137.

Tustison, N.J., Avants, B.B., Cook, P.A., Zheng, Y., Egan, A., Yushkevich, P.A., Gee, J.C., 2010. N4ITK: improved N3 bias correction. IEEE Trans. Med. Imaging 29 (6), 1310. doi:10.1109/TMI.2010.2046908.N4ITK.

Tustison, N.J., Cook, P.A., Klein, A., Song, G., Das, S.R., Duda, J.T., Kandel, B.M., van Strien, N., Stone, J.R., Gee, J.C., Avants, B.B., 2014. Large-scale evaluation of ANTs and FreeSurfer cortical thickness measurements. NeuroImage 99, 166–179. doi:10.1016/j.neuroimage.2014.05.044.

Van Essen, D.C., Dierker, D.L., 2007. Surface-based and probabilistic atlases of primate cerebral cortex. Neuron 56, 209–225. doi:10.1016/j.neuron.2007.10.015.

Wang, Y., Nie, J., Yap, P.T., Li, G., Shi, F., Geng, X., Guo, L., Shen, D., 2014. Knowledge-guided robust MRI brain extraction for diverse large-scale neuroimaging studies on humans and non-human primates. PLoS One 9, 1–23. doi:10.1371/journal.pone.0077810.

Whelan, C.D., Altmann, A., Botía, J.A., Jahanshad, N., Hibar, D.P., Absil, J., Alhusaini, S., Alvim, M.K.M., Auvinen, P., Bartolini, E., Bergo, F.P.G., Bernardes, T., Blackmon, K., Braga, B., Caligiuri, M.E., Calvo, A., Carr, S.J., Chen, J., Chen, S., Cherubini, A., David, P., Domin, M., Foley, S., França, W., Haaker, G., Isaev, D., Keller, S.S., Kotikalapudi, R., Kowalczyk, M.A., Kuzniecky, R., Langner, S., Lenge, M., Leyden, K.M., Liu, M., Loi, R.Q., Martin, P., Mascalchi, M., Morita, M.E., Pariente, J.C., Rodríguez-Cruces, R., Rummel, C., Saavalainen, T., Semmelroch, M.K., Severino, M., Thomas, R.H., Tondelli, M., Tortora, D., Vaudano, A.E., Vivash, L., von Podewils, F., Wagner, J., Weber, B., Yao, Y., Yasuda, C.L., Zhang, G., Bargalló, N., Bender, B., Bernasconi, N., Bernasconi, A., Bernhardt, B.C., Blümcke, I., Carlson, C., Cavalleri, G.L., Cendes, F., Concha, L., Delanty, N., Depondt, C., Devinsky, O., Doherty, C.P., Focke, N.K., Gambardella, A., Guerrini, R., Hamandi, K., Jackson, G.D., Kälviäinen, R., Kochunov, P., Kwan, P., Labate, A., McDonald, C.R., Meletti, S., O'Brien, T.J., Ourselin, S., Richardson, M.P., Striano, P., Thesen, T., Wiest, R., Zhang, J., Vezzani, A., Ryten, M., Thompson, P.M., Sisodiya, S.M., 2018. Structural brain abnormalities in the common epilepsies assessed in a worldwide ENIGMA study. Brain 141, 391–408. doi:10.1093/brain/awx341.

Wierenga, L.M., Langen, M., Oranje, B., Durston, S., 2014. Unique developmental trajectories of cortical thickness and surface area. NeuroImage 87, 120–126. doi:10.1016/j.neuroimage.2013.11.010.

Yc, K., Prado, L., Merchant, H., 2019. The scalar property during isochronous tapping is disrupted by a D2-like agonist in the nonhuman primate. J. Neurophysiol. 121, 940–949. doi:10.1152/jn.00804.2018.

Young, J.T., Shi, Y., Niethammer, M., Grauer, M., Coe, C.L., Lubach, G.R., Davis, B., Budin, F., Knickmeyer, R.C., Alexander, A.L., Styner, M.A., 2017. The UNC-Wisconsin rhesus macaque neurodevelopment database: a structural MRI and DTI database of early postnatal development. Front. Neurosci. 11, 29. doi:10.3389/fnins.2017.00029.

Zhong, J., Phua, D.Y.L., Qiu, A., 2010. Quantitative evaluation of LDDMM, FreeSurfer, and CARET for cortical surface mapping. NeuroImage 52, 131–141. doi:10.1016/j.neuroimage.2010.03.085.

Zhou, D., Lebel, C., Evans, A., Beaulieu, C., 2013. Cortical thickness asymmetry from childhood to older adulthood. NeuroImage 83, 66–74. doi:10.1016/j.neuroimage.2013.06.073.